Title: Collaborative Cross mice have diverse phenotypic responses to infection with Methicillin-resistant *Staphylococcus aureus* USA300.

Short Title: MRSA Infection in CC mice

Authors: Aravindh Nagarajan[1,3], Kristin Scoggin[1,3], Jyotsana Gupta[3], Manuchehr Aminian[6,7], L. Garry Adams[8], Michael Kirby[6], David Threadgill[1,2,4,5], Helene Andrews-Polymenis [1, 3] *

Affiliations

[1]Interdisciplinary Program in Genetics and Genomics, Texas A&M University, College Station, Texas, United States of America

[2]Department of Molecular and Cellular Medicine, Texas A&M University, College Station, Texas, United States of America

[3]Department of Microbial Pathogenesis and Immunology, Texas A&M University, College Station, Texas, United States of America

[4]Texas A&M Institute for Genome Sciences and Society, Texas A&M University, College Station, Texas, United States of America

[5]Department of Biochemistry & Biophysics and Department of Nutrition, Texas A&M University, College Station, Texas, United States of America

[6]Department of Mathematics, Colorado State University, Fort Collins, Colorado, United States of America

[7]Department of Mathematics and Statistics, California State Polytechnic University, Pomona, California, United States of America

[8]Department of Veterinary Pathobiology, Texas A&M University, College Station, Texas, United States of America

*Corresponding author

Keywords: Host-pathogen interaction, MRSA USA300, Collaborative Cross, QTL mapping, *Npc1*, *Ifi44l*, tolerance, sepsis, sex-difference in infection

Abstract:

Staphylococcus aureus (*S. aureus*) is an opportunistic pathogen causing diseases ranging from mild skin infections to life-threatening conditions, including endocarditis, pneumonia, and sepsis. To identify host genes modulating this host-pathogen interaction, we infected 25 Collaborative Cross (CC) mouse strains with methicillin-resistant *S. aureus* (MRSA USA300) and monitored disease progression for seven days. We identified eight 'susceptible' CC strains with high bacterial load, tissue damage, and reduced survival. Among the surviving strains, six with minimal colonization were classified as 'resistant', while the remaining six tolerated higher organ colonization ('tolerant'). The kidney was the most heavily colonized organ, but liver colonization was better correlated with reduced survival. We identified four CC strains with sex differences: females survived the study period while males met our euthanasia criteria earlier. In these CC strains, males had more baseline circulating monocytes and red blood cells. We identified several CC strains that may be useful as new models for endocarditis, myocarditis, pneumonia, and resistance to MRSA infection. Resistant strains had higher pre-infection circulating neutrophils than susceptible and tolerant strains. GM-CSF, IL-1-alpha, IL-15, IL-28, and IL-31 levels increased significantly in tolerant strains after infection. Using RNA seq, we identified two pathways, IL-1 and ERK1/ERK2, as potentially involved in the mechanism of tolerance. QTL analysis identified two significant loci, on Chromosomes 18 and 3, involved in early and late survival after infection. We prioritized *Npc1* and *Ifi44l* genes as the strongest candidates influencing survival using variant analysis and mRNA expression data within these intervals.

Author Summary:

Methicillin-resistant *Staphylococcus aureus* (MRSA) is a human opportunistic pathogen that can cause life-threatening diseases. To study the influence of host genetics on the outcome of MRSA infection, we infected a collection of genetically diverse mice. We identified different phenotypes for survival, organ colonization, and tissue damage, and classified CC strains into MRSA susceptible, tolerant, and resistant categories. Four CC strains had strong sex differences in infection outcome: females lived longer, and males had higher baseline circulating monocytes and red blood cells. Several of the CC strains we characterize may represent better animal models for diseases caused by MRSA. Resistant and tolerant strains appear to have different immunologic states both pre-infection and in response to infection. QTL analysis identified two genes, *Npc1* and *Ifi44l*, as strong candidates for involvement in early and late survival after MRSA infection. Our data suggests a strong involvement of host genetics in MRSA infection outcome.

Introduction

Staphylococcus aureus, a gram-positive pathogen, is a commensal organism and opportunistic pathogen that can cause severe morbidity and mortality [1, 2]. This organism colonizes 20-30% of humans permanently and another 50-60% intermittently [3, 4]. *S. aureus* is a multi-host pathogen that can colonize and cause disease in cows, chickens, pigs, sheep, and wild animals [5]. A range of conditions, from skin and soft tissue infections to severe life-threatening diseases, including sepsis and toxic shock syndrome, can result from *S. aureus* infection [6]. *S. aureus* is the leading cause of bacteremia, skin and soft tissue infections, bone and joint infections, and hospital-acquired infections [7].

Methicillin-resistant *S. aureus* (MRSA) is a strain of *S. aureus* resistant to β-lactam antibiotics [8]. MRSA was first described in the early 1960s and was primarily associated with hospital-acquired infections until the 1980s [9, 10]. In the 1990s, MRSA started spreading rapidly in the community and is now considered a global threat [7]. The World Health Organization (WHO) reported that people with MRSA are 64% more likely to die than people with drug-sensitive infections (WHO, 2018). MRSA causes more than 300,000 hospitalizations and 10,000 deaths in the US annually, at an estimated healthcare cost of 1.7 billion dollars (CDC, 2018).

USA300 is a highly successful community-acquired clone of MRSA. First reported in 1999, by 2011 USA300 had become the primary cause of severe skin and soft-tissue infections, bacteremia, and community-onset pneumonia [11]. The increased disease burden caused by MRSA USA300 is attributed to the presence of multiple mobile genetic elements (MGEs) carrying virulence factors. These virulence factors

include Panton-Valentine Leukocidin (PVL) gene, Arginine-Catabolic Mobile Element (ACME), Enterotoxins K and Q, Staphylococcal cassette chromosome *mec* type IV (SCC mec IVa), and fluoroquinolone resistance acquired through mutations in *gyrA* and *grlA* [12, 13]. In humans, USA300 infections are associated with increased mortality and increased incidence of severe sepsis than hospital-acquired MRSA infections [14, 15]. This hypervirulence exhibited by USA300 over other strains has been repeatedly demonstrated in several animal models [16-18].

Mouse models have helped identify susceptibility genes and understand the mechanism of pathogenesis of many bacterial pathogens and diseases [19]. *S. aureus* infections in mice induce a diverse spectrum of diseases similar to what is observed in humans [20]. Intravenous infection with *S. aureus* in mice is commonly used as a model for sepsis with this pathogen [20-23]. Mice lacking MyD88 (myeloid differentiation primary response protein), a cytoplasmic adaptor involved in the IL-1R (Interleukin-1) and TLR-2 (Toll-Like Receptor 2) pathways, are highly susceptible to *S. aureus* intravenous infections [24]. Similarly, mice deficient in NOD2 (nucleotide-binding oligomerization domain-containing protein 2) are more susceptible to intraperitoneal infection with *S. aureus* [25].

Outcomes after infection with *S. aureus* differ depending on the strain of laboratory mice used. In a bacteremia model, C57BL/6 mice are the most resistant in controlling bacterial growth and survive, while A/J, DBA/2, and BALB/c mice are highly susceptible [26]. This information has been used to map genetic loci involved in this differential outcome. Using C57BL/6J and A/J Chromosomal substitution strains (CSS), six genes on three different chromosomes (Chr 11 – *Dusp3*, *Psme3*; Chr 8 – *Crif1,*

Cd97; Chr 18 – *Tnfaip8, Seh1l*) have been implicated to susceptibility after infection with *S. aureus* (sanger 476) strain [27-29].

Collaborative Cross (CC) mice have been successfully used to create disease models and identify susceptibility genes for various infections [30]. The CC is a large panel of recombinant inbred mouse strains created by interbreeding five classical inbred strains (A/J, C57BL/6J, 129S1/SvlmJ, NOD/ShiLtJ, NZO/HlLtJ) and three wild-derived inbred strains (CAST/EiJ, PWK/PhJ, and WSB/EiJ) using a funnel-breeding scheme [31, 32]. CC strains have more than 30 million Single Nucleotide Polymorphisms (SNPs), and their genomes are fully sequenced, making them an ideal population for Quantitative Trait Locus (QTL) mapping [33, 34]. The CC has been heavily used to identify susceptibility to viral pathogens, including Ebola virus [35], West Nile virus [36], Influenza A virus [37], Coronaviruses [38, 39], Theiler's murine encephalomyelitis virus [40], Cytomegalovirus [41] and Rift Valley fever virus [42]. The CC has also been used to study infection with bacterial pathogens, including *Mycobacterium tuberculosis* [43, 44], *Klebsiella pneumonia* [45], *Pseudomonas aeruginosa* [46], *Borrelia recurrentis* [47], *Salmonella* Typhimurium [48, 49] and *Salmonella* Typhi [50].

We infected 25 CC strains intravenously with MRSA USA300 to study disease outcomes across diverse host genetics. We monitored infected mice for clinical symptoms using telemetry and a manual health scoring method for up to one-week post-infection. Organs and blood were collected at necropsy to quantify colonization, tissue damage, complete blood counts (CBC), and cytokine levels. We observed a wide range in survival and weight loss after infection. The kidney was the most highly colonized organ, but liver colonization was more highly correlated with poor survival.

Four strains exhibited sex differences in survival: infected females lived until the end of the experiment (day 7), but all the males met our euthanasia criteria much earlier. Several CC strains we characterized could be used as new models for studying endocarditis, myocarditis, pneumonia, and resistance to MRSA infection. We also prioritized several blood, cytokines, and immune pathways that differentiated the tolerance from resistance. QTL analysis identified two significant genomic loci involved in early and late survival after infection. Shortlists of the strongest candidate genes within these intervals were generated using variant analysis and mRNA expression data.

Results

CC strains exhibit diverse responses to MRSA infection.

We infected twenty-five Collaborative Cross (CC) strains (three males and three females per strain) with MRSA USA300 (Table S1). Animals were monitored for clinical symptoms using a telemetry system and a manual health scoring method up to one-week post-infection to identify those susceptible to MRSA infection. C57BL/6J (B6) mice, known to survive MRSA infection, served as negative controls. At the time of necropsy spleen, liver, heart, lung, and kidney were collected to enumerate the bacterial load (Table S2).

All C57Bl6 mice survived until the end of the experiment (day 7) and were classified as a surviving strain (Fig 1A). C57Bl6 mice lost a median of 8.90% of their body weight and had high kidney colonization (Fig 1B and Fig 1C). CC strains that had four or more mice of the six infected meeting our euthanasia criteria before day seven

were classified as ‘susceptible’. Eight of the 25 CC strains we infected were classified in this category (CC053, CC027, CC037, CC036, CC061, CC006, CC057, CC002, Fig 1A).

Five CC strains had three mice that met our euthanasia criteria before day 7. Of these five strains, four showed sex-dependent survival: all the males met our euthanasia criteria early in the experimental period, while all females of these strains survived the full 7-day infection period. These four CC strains were classified as sex-difference strains (CC013, CC058, CC043, CC015, Fig 1A). CC042 couldn’t easily be classified, as two females and one male survived MRSA infection.

We classified the remaining 12 surviving CC strains into tolerant and resistant phenotypes. Tolerance was defined as surviving the infection with a high bacterial burden. Surviving the infection by preventing colonization or clearing the pathogen was defined as resistance. Six strains with higher total organ colonization compared to the inoculum dose were classified as tolerant (CC019, CC005, CC001, CC024, CC051, CC038). The remaining six strains, with minimal or no colonization, were classified as resistant (CC023, CC025, CC012, CC003, CC041, CC017) (Fig 1 and Fig S1).

Pre-infection weight did not influence survival (R = -0.05), while weight loss after infection correlated with poor survival (R = -0.65) (Fig S2). Susceptible strains, on average, lost 16% of their body weight, while tolerant and resistant strains lost 7% and 5%, respectively (Fig 1B). Colonization in all five organs highly correlated with each other (Fig S2). 10 mice belonging to 6 different strains had no colonization across the organs collected (Fig 1 and Fig S1). We included them in the analysis based on

disturbances in circadian pattern following infection, suggesting that they did become infected, as well as histology scores. The kidney was the highest colonized organ across all CC strains and high kidney colonization correlated with poor survival (R = -0.58) (Fig S2). Two susceptible strains, CC027 and CC057, had median kidney colonization on the order of 10^9, ~100-fold higher than the inoculation dose. Several resistant strains, including CC012, CC025, CC003, and CC017, had lower or no MRSA colonization of the kidneys (Fig 1C).

The inability to limit bacterial growth in the kidney is associated with susceptibility to intravenous *S. aureus* infections in mice [26]. In the CC strains we screened, colonization in the liver (R = -0.78), spleen (R = -0.73), and lung (R = -0.67) was more highly correlated with poor survival than colonization of the kidneys (Fig S2). Heart and kidney colonization were similarly correlated with survival (R = -0.58) (Fig S2). Furthermore, liver colonization had a high positive correlation with spleen (R = 0.79), lung (R = 0.78), and heart (R=0.67) colonization (Fig S2). These data suggest that several CC strains tolerated high kidney colonization but reached our euthanasia criteria when the pathogen load increased in other organs. The diverse response of CC strains to MRSA infection is evident in the wide range of disease severity, survival, weight loss, and organ colonization we observed.

<u>Survival is sex-dependent in four CC strains.</u>

A sex difference in survival was defined as only males or females within a strain surviving the infection to day 7. Four strains, CC013, CC015, CC043, and CC058, met this criterion for sex differences (Fig 1A). In these four strains, females lived until the

end of the experiment (day 7), but all the males met our euthanasia criteria much earlier (Fig 2A). After removing these four strains and looking at the remaining CC mice (21 strains) as a population, there was no significant difference in survival (P = 0.51) and weight change after infection (P = 0.13) between males and females (Table S2).

In the four sex difference strains, males lost more weight than females (Fig 2B) and had higher liver, spleen, and lung colonization (Fig 2C). Colonization did not significantly differ between males and females in the kidneys, the highest colonized organ in these strains (Fig 2C). Females in these CC strains appear to limit MRSA spread from the kidneys and/or bacterial replication in other vital organs by an unknown mechanism.

To assess baseline differences between males and females of the sex difference strains, we evaluated pre-infection complete blood counts (CBC). Interestingly, males had higher circulating levels of monocytes and red blood cells before infection than females of these strains (Fig 2D). The number of circulating monocytes (P = 0.83) and red blood cells (P = 0.10) were not significantly different between males and females in the rest of the CC population (21 strains) (Table S2). Thus, this difference in the starting blood parameters is unique to CC strains that displayed sex differences in susceptibility to MRSA infection.

<u>Tissue damage correlates poorly with survival</u>

A board-certified pathologist scored each tissue blindly for damage using a scale of 0 to 4 (0 = normal to 4 = severe damage) (Table S3 and Fig S3). Tissue damage in three of the five organs we examined had a weak correlation with poor survival (Fig S2).

Spleen damage had the highest correlation with R = -0.23, followed by the kidney (R = -0.18) and heart (R = -0.18) damage. This weak correlation may be due to the diverse phenotypic responses exhibited by the CC strains to MRSA infection. Some infected CC strains met our euthanasia criteria very early in infection, perhaps before extensive tissue damage had time to occur. Other CC strains lived to the end of the experiment, allowing time for severe tissue damage to occur and become cumulative (Fig 3).

However, high colonization in kidneys translated to more significant tissue damage. Of the 25 CC strains we studied, 16 had a median pathology score of 2.5 or above for kidneys, indicating moderate to severe tissue damage (0=normal tissue, 4= severe damage) (Table S2). Two strains, CC017 and CC043, had no visible kidney damage (Fig 3). CC017 is a resistant strain explaining minimal tissue damage in the kidneys and other organs. But CC043 mice were highly colonized across all organs and lost more than 10% of their body weight, although this strain had a sex difference with the females resistant to MRSA infection (Fig 1 and S1).

For tissue damage, across all the organs, resistant strains had significantly less damage than tolerant strains ($P < 0.001$) and susceptible strains ($P < 0.010$). Interestingly, there was no significant difference in tissue damage as blindly scored by a board-certified pathologist, between tolerant and susceptible strains ($P = 0.57$). CC042 and CC036 mice had severe damage in their hearts. Histologic examination revealed that this damage was purulent bacterial myocarditis and myocardial necrosis. Sex difference strains varied widely in tissue damage scores. Both males and females in CC013 and CC058 had damage across all the tissues, despite the fact that females of

these strains survived while the males did not. CC043 did not have any damage in either sex.

Baseline body temperature and baseline activity did not correlate with survival.

A surgically implanted telemetry device tracked body temperature and activity levels every minute before and throughout the infection. Data from five days before infection was used to create a baseline circadian pattern for each mouse using a machine-learning algorithm. A machine-learning algorithm was also used to predict when infected mice deviated from their normal circadian pattern of body temperature and activity after infection. No significant differences were identified in the elapsed time between infection and deviation from the normal circadian pattern between surviving and susceptible strains. 90% of the infected mice deviated from their normal circadian pattern of body temperature and activity within 24 hours of infection (Fig S4). The first health check performed by laboratory staff, 24 hours after infection, could only detect 56% of these mice. In the next two days, twice daily health checks detected all the remaining mice as ill (Fig S4). These data suggest a significant lag time between circadian pattern disruption detected by telemetry and signs of illness detected by laboratory staff.

Immune parameters that differ between phenotypes.

Blood was collected from mice five weeks before the infection by cheek bleed, and at necropsy, whole blood and serum were collected. Complete blood counts (CBC) were determined using an automated CBC machine, and circulating cytokine levels were determined from serum using a 36-plex cytokine/chemokine panel. To account for

baseline differences in CBC parameters across the CC strains, we determined the change in each parameter after infection by subtracting post-infection CBC values from pre-infection values from the same animal. Post-infection cytokine/chemokine values were subtracted by values from age and sex-matched uninfected animals from the same CC strains.

CC strains resistant to MRSA infection had a higher number of pre-infection circulating neutrophils than susceptible and tolerant strains (Fig 4A). There were no significant differences in other pre-infection CBC parameters (Table S2). Post-infection, we only looked at the differences between tolerant and resistant strains, as both groups were euthanized at the same time point (Day 7 post infection). Platelet indices, platelet distribution width (PDW), and mean platelet volume (MPV) increased in tolerant strains after infection (data not shown). Increases in these platelet parameters suggest platelet activation is occurring in MRSA tolerant CC strains [51, 52]. Among the 36 cytokines and chemokines we measured, only five differed significantly between the tolerant and resistant strains. GM-CSF, IL-1-alpha, IL-15, IL-28, and IL-31 were significantly elevated in tolerant strains compared to resistant strains (Fig 4B).

Kidneys were collected during the necropsy and were used for RNA sequencing. 152 genes were differentially expressed between the tolerant and the resistant strains. Of these, 88 were up-regulated in tolerant strains, and 64 were down-regulated (Fig S5A). Differentially expressed genes were analyzed for the enrichment of biological processes. Down-regulated genes were primarily involved in metabolism and electron transport chain, significantly affecting normal cell activities. All up-regulated genes were involved in immune-related pathways (Fig 4C). Homotypic cell-cell adhesion and

response to IL-1 were the top two enriched pathways. These processes, up-regulated in tolerant strains, grouped into the ERK1/ERK2 cascade, response to IL-1, response to cytokines, and innate and adaptive immune responses in enrichment tree analysis (Fig S5B).

Two independent genomic regions influence survival.

We used a modified version of RQTL2 and qtl2qpi to identify chromosomal regions associated with survival after MRSA infection [53, 54]. We used the number of mice within a strain that survived at the end of each day as the phenotype. For a successful QTL analysis, a phenotype needs to be highly heritable. Within the CC strains we infected, survival was a highly heritable trait with a broad sense heritability score of 0.38. When sex was included as a cofactor, heritability increased to 0.63. For early survival on day 2, there was a highly significant peak on chromosome 18 (Fig 5A). We named this QTL peak ESMI (Early Survival in MRSA Infection). This peak disappeared after day 3 post-infection.

For survival until day 7 (late survival), there was a highly significant peak on Chromosome 3 (Fig 5B). We named this peak LSMI (Late Survival in MRSA Infection). To understand the impact of sex on survival, we performed the same analysis after removing the four strains that exhibited sex differences in survival. The early survival peak on Chr 18 and late survival peak on Chr 3 were retained (Fig S6), suggesting that sex did not influence our QTL peaks. We compared the phenotype at the top SNPs in both peaks for potential interaction. We did not identify any significant interactions, suggesting that our QTL regions act independently of each other.

Npc1 is a candidate gene for early survival during MRSA infection.

The advantage of CC panel over other outbred mouse panels is the high number of SNPs and structural variants present across the CC genomes [33, 34]. We used this feature to shortlist the genes within the associated genomic regions to identify those of most interest. The early survival QTL peak, ESMI, on chromosome 18 is a 5 Mb region between 12-17 Mb with a peak around 14.67 Mb. This region contains 21 protein-coding genes and 49 non-coding RNA genes. Because the CC strains are a mosaic of eight inbred founder strains, we looked at the founder effect plot in this region to attempt to identify each founder's contribution to survival. We found that the WSB allele contributes to reduced survival, while A/J and NZO alleles contribute to prolonged survival (Fig 6A). Using all the SNPs, insertions and deletions that matched this allele effect pattern using the Mouse Phenome Database (MPD), we identified 20,582 variants spread across all 21 genes. We used Variant Effect Predictor (VEP) to further prioritize these variants based on their predicted effect on protein structure and function, identifying 52 high and moderate-impact variants in 7 genes (Table S4). The highest impact variant for each gene is listed (Fig. 6B). Four of the seven genes we shortlisted have previously been associated with immune function in the Mouse Genome Informatics Portal (highlighted in red) [55]. We sequenced mRNA from kidneys collected from CC strains at necropsy (at least one male and one female per strain) to further prioritize genes. Then, we looked for differentially expressed genes that matched the founder effect pattern within this region. For the early survival QTL peak, two genes, *Npc1* and *Cdh2*, matched the founder effect pattern (Fig 7C). *Npc1* is our top candidate in this region due to its previous association with the immune system.

Ifi44l is a strong candidate for involvement in late survival after MRSA infection.

The late survival QTL peak, LSMI, on chromosome 3 is a 4 Mb region between 146-150 Mb with a peak near 146.66 Mb. This region contains 13 protein-coding genes and 39 non-coding RNA genes. The A/J allele significantly reduced survival, while CAST, NOD, NZO, and WSB alleles promoted longer survival (see founder effect plot, Fig 7A). Using this founder effect pattern, we shortlisted five genes with variants predicted to have a high impact on the function of the encoded proteins (Table S4). The top variant for each gene is listed (Fig 7B). Gene expression data narrowed our shortlist to *Ifi44l*, a gene that is highly expressed in strains with the A/J allele but not with the alleles from the other founders (Fig 7C).

QTL analysis for other phenotypes.

We collected a large amount and variety of data throughout this experiment and wanted to utilize as much of this data as possible. Therefore, in addition to using the survival data, we performed QTL analysis for 188 other phenotypes. These phenotypes included weight change, circadian parameters, nestlet scores, CBC, and cytokine/chemokine values, before and after MRSA infection. At an 85% significance level, we detected 39 QTL peaks for 36 parameters (by permutation testing see Materials and Methods, Table S5). The median 1.8 drop interval for these peaks was 6.12 Mb. We focused on the 15 peaks that passed the significance at the 95 % level for variant shortlisting (Table S5). We generated the founder effect and phenotype-genotype plot for each QTL peak (Fig S7). Using the Mouse Phenome Database (MPD), we shortlisted high-impact genes in these intervals that matched the founder effect

pattern (Table S6).

Discussion

Staphylococcus aureus (*S. aureus*) is a highly successful organism that colonizes approximately one-third of the human population asymptomatically [3]. *S. aureus* colonization is a risk factor for subsequent infections ranging from mild skin and soft tissue infections to serious invasive infections and death [56, 57]. *S. aureus* has a complex repertoire of virulence factors, pathogenicity islands, and toxins and has developed resistance to multiple antibiotics [9]. Many studies have focused on understanding the genetics of *S. aureus* pathogenesis, but the host genetic factors that modulate this host-pathogen interaction are poorly studied. We infected 25 genetically diverse CC mouse strains with MRSA USA300 to find the host genetic factors contributing to disease susceptibility or resistance over a 7-day infection.

CC strains vary widely in their response to MRSA sepsis. Survival ranged from 2.5 to 7 (end of the experiment) days. Weight loss ranged from strains losing 20% of their body weight (CC037, CC002) to strains losing less than 1% (CC017, CC003, CC024). The kidney is one of the primary organs for MRSA colonization in mice and was the highest colonized organ in our study [26, 58], yet across CC strains, kidney colonization varied widely. In CC strains, high liver, spleen, and lung colonization correlated more closely with poor survival than did kidney colonization (Fig S2). Kupffer cells, specialized liver macrophages, are essential for the initial clearing of *S. aureus* from the bloodstream [59, 60]. Perhaps high MRSA colonization in the liver overwhelms

the ability of resident Kupffer cells to clear MRSA, contributing to the correlation between liver colonization correlates and poor survival in CC strains.

We identified 8 CC strains that were susceptible to MRSA sepsis based on reduced survival after infection. Within these susceptible strains, the phenotypic response was diverse. Survival ranged from 2.5 to 4 days, and kidney colonization varied as much as 10-fold. CC061 and CC036 had very similar kidney colonization, yet CC061 appeared to have a more severe disease and lost twice as much weight as CC036 (19% vs. 9%). We observed similar diversity in weight loss and colonization within tolerant and resistant phenotypes as well. These data suggest that multiple mechanisms of susceptibility, tolerance and resistance to MRSA infection exist across a broad set of host genetics.

The majority of the CC strains used in this study were also used to define susceptibility to non-typhoidal *Salmonella* infection [48, 49]. Of the eight MRSA susceptible strains, six were also classified as susceptible or delayed susceptible to *Salmonella* infection (CC053, CC027, CC037, CC036, CC061, CC006). The two remaining MRSA susceptible strains, CC057 and CC002, were classified as resistant and tolerant to *Salmonella* infection, respectively [49]. CC038 was classified as tolerant to both MRSA and *Salmonella* infection. None of the other MRSA tolerant or resistant strains matched the *Salmonella* response classification.

We also compared MRSA infection outcome data to another study of *Mycobacterium tuberculosis* (Mtb) infection in CC strains [44]. This study did not classify survival phenotypes, so we used the median lung colonization values for each strain for comparison to our survival data. For the 52 CC strains infected with Mtb, log lung CFU

ranged from 5.1 to 8.5, with a median of 6.7 CFU. Among the six MRSA-susceptible strains, two strains, CC061 and CC006, had very low lung CFU (5.6 and 6.5 log CFU) when infected with *Mtb*. On the other hand, three other susceptible strains, CC037, CC027, and CC002, had very high lung colonization with *Mtb* (average – 8.2 log CFU). Two of these strains, CC027 and CC037, were sensitive to both *Salmonella* and MRSA infection and were also heavily colonized in the lung with *Mtb* [44, 48, 49]. These data suggest that in these two CC strains, sensitivity to three different bacterial pathogens may be occurring through a common mechanism.

All five MRSA-resistant CC strains when infected with *Mtb* had very high colonization in the lung (average – 8.4 log CFU), suggesting these strains were likely susceptible to *Mtb* infection. CC038, classified as tolerant to MRSA and *Salmonella*, is also likely tolerant to *Mtb* infection with a lung CFU of 7.3, close to the median lung colonization across all CC strains. The other MRSA-tolerant strains had variable *Mtb* CFU in the lungs. This differential response of CC strains to different bacterial pathogens suggests that most CC strains that we used do not have a significant general dysfunction of immunity, where we would expect broad susceptibility to multiple pathogens.

In both animals and humans, males are more susceptible than females to bacterial infections [61]. Some of these differences can be attributed to the differences in X-chromosome number and inactivation process between males and females. The X-chromosome also encodes several critical immune genes, including interleukin-1 (IL-1) receptor-associated kinase 1 (IRAK1), Colony-stimulating factor 2 receptor α (CSF2RA), IL-2 receptor-γ chain, IL-3 receptor-α chain, IL-9 receptor, Toll-like receptor 7 (TLR7),

TLR8, and FOXP3, that could play important roles in sex differences in infection outcome [62]. Males have a higher overall risk for MRSA carriage [63] and bloodstream infections [64, 65]. However, there is no consensus on the role of gender in the mortality rate. Several studies have found higher mortality in females [66-68], while other studies have reported no association of mortality with gender [65, 69].

In our total study population, females survived longer than males, but this sex difference was driven by 4 CC strains that exhibited strong sex differences in survival. Within the strains with sex differences in survival, males lost more weight and were colonized more heavily in the liver, spleen, and lung than females. We examined the blood parameters of male and female uninfected mice of these CC strains to identify baseline differences. Two blood parameters, circulating monocytes (MON) and red blood cells (RBC), were higher in males of these strains prior to infection (Fig 2D) but were not significantly different between the sexes in the rest of the CC population.

While the reason why these blood parameters vary must be further investigated, *S. aureus* has a repertoire of virulence factors to take advantage of these parameters in males. *S. aureus* persists within monocyte-derived macrophages and can use these cells as a vehicle for further dissemination [70, 71]. Similarly, S *aureus* can bind directly to both RBCs [72-74] and hemoglobin [75] and possesses multiple virulence factors to lyse erythrocytes [76]. Additionally, heme iron is the preferred source of iron for *S. aureus* during infection [77]. Increased pre-infection levels of monocytes may serve as a mechanism for more efficient MRSA dissemination and increased RBC and hemoglobin may serve as nutrient source during infection in males of some CC strains.

One of the advantages of using a panel of genetically diverse inbred mice is the ability to identify mouse strains for model generation. MRSA is well adapted to multiple hosts and can cause diverse diseases but studying these diseases in humans is heavily confounded by environmental factors and comorbidities [20, 78, 79]. Thus, studies investigating the pathogenesis of *S. aureus* have relied heavily on mouse models [80]. The four sex-difference strains we identified are ideal candidates for investigating the role of sex/gender in MRSA infection outcomes.

S. aureus is the leading cause of infective endocarditis (IE), which results in high mortality (40-50%) [81, 82]. Current mouse models of IE require anesthetizing mice and physically damaging the heart valve using a catheter prior to *S. aureus* infection [83]. C57BL6 mice are typically used as background strains for the IE model [84]. *S. aureus* is also the most common cause of rare bacterial myocarditis, with fatal outcomes in some cases [85-87]. Currently, there are no murine models to study MRSA induced myocarditis. In our study, three CC strains, C0042, CC013, and CC036, had over 200-fold greater colonization in the heart compared to C57BL6 mice. and CC042 and CC013 also had severe tissue damage in the heart . On histological examination, we observed systemic embolic bacterial purulent myocarditis. CC042 and CC013 may be useful for studying cardiac disease due to MRSA without the need to physically damage heart valves prior to infection. Similarly, pneumonia caused by *S. aureus* has a high mortality rate [88]. In our study, CC013, CC058, and CC061, had significant lung damage and could perhaps be used for studying *S. aureus* pneumonia. C57BL6 mice are the most resistant mouse strain to *S. aureus* infection in the literature [26, 29], but do not clear the pathogen completely.

We identified six resistant CC strains that both survive MRSA infection and have lower bacterial colonization than C57BL6 mice (Fig 1 and S1). Most of these strains also had less tissue damage than C57BL6 mice (Fig 3). These resistant strains are ideal candidates for future studies investigating the mechanisms of resistance to *S. aureus* infection.

Changes in body temperature and activity are important clinical signs for disease diagnosis and prognosis. During the recent COVID-19 pandemic, there was an increased emphasis on using changes in body temperature to detect illness all over the world [89, 90]. The reliability of using body temperature to screen patients with COVID-19 illness has been questioned [91, 92]. Using an implanted telemetry device, we measured the core body temperature and activity of each animal in our study. We found that both daytime and nighttime baseline body temperatures medians were quite variable. The diversity in these thermal patterns across CC strains should prompt caution when interpreting a single measurement of body temperature as an indicator of illness in mice. Furthermore, pre-infection temperature and activity were highly heritable, suggesting the involvement of a genetic component. Unfortunately, we did not identify significant peaks in our QTL analysis for these parameters likely due to use of a limited number of animals.

Pre-infection inflammation and immune parameters play a role in disease prediction and progression [39, 93]. Among all the CBC parameters we compared, pre-infection circulating neutrophil numbers were significantly higher in MRSA resistant strains than in the tolerant and susceptible strains. Neutrophils are the primary defense against *S. aureus* infections [57, 94], and patients with impaired neutrophil numbers and

function are predisposed to *S. aureus* infections [95-97]. The high pre-infection circulating neutrophil numbers in the MRSA-resistant CC is consistent with this human data and may decrease colonization by MRSA in these strains.

S. aureus evades phagocytosis by modifying its cell surface and producing a repertoire of virulence factors [98, 99]. These factors aid in both evading and attacking the host immune system. We found increases in GM-CSF, IL-1α, IL-15, IL-28, and IL-31 levels in tolerant strains compared to the resistant strains. GM-CSF and IL-1α recruit neutrophils and up regulate their properties to clear pathogens [100-102]. Tolerant strains appear to be actively recruiting neutrophils to clear MRSA.

However, IL-28, IL-15, and IL-31 may help *S. aureus* persist, but these effects have not been demonstrated in models of septic infection. Mice lacking the receptor for IL-28 clear *S. aureus* better and have less pulmonary pathology [103]. Similarly, mice lacking IL-15 have improved clearance of *S. aureus* in a mouse arthritis model [104], and IL-31 supplementation enhanced *S. aureus* colonization in an epidermal model [105]. Further studies will tease out the role of these cytokines in the tolerance phenotype during systemic MRSA infection.

The two pathways up-regulated in tolerant strains in our gene expression analysis are IL-1 and the ERK1/ERK2 cascade (Fig 4C and S4B). In humans, mutations in the IL-1 pathway lead to increased susceptibility to some bacterial infections, particularly streptococcal and staphylococcal infections [106]. Activation of the IL-1 receptor (IL-1R) via the secretion of IL-1α and IL-1β activates the MyD88/IRAK4 pathway, resulting in the production of cytokines and chemokines promoting neutrophil recruitment and pathogen clearance [107]. In *S. aureus* septic infections, IL-1R deficient

mice have increased mortality [108], and blocking the IL-1 receptor increased susceptibility in mice [101]. In our experiments, IL-1α levels are increased in the serum of tolerant strains (Fig 4B). Thus, the IL-1 pathway appears to play a critical role in the survival of MRSA-tolerant strains, potentially causing increased neutrophil recruitment.

The extracellular signal-regulated kinase 1/2 (ERK1/2) signaling pathway regulates cell proliferation, differentiation, and survival during stress response [109]. ERK1/2 molecules are expressed in very large quantities (~10^7 molecules/cell) and bind more than 200 distinct substrates in the cell [110]. Although ERK 1/2 enters the nucleus and alters gene expression of several transcription factors, including NF-κB, its role in bacterial infections is poorly understood [111]. ERK1/2 inhibitors have been successfully used to increase survival in mouse models of *S. aureus* sepsis [112, 113], but their mechanism of action is not clearly known. Future studies will be needed to identify the mechanism of ERK1/2 pathway participation in the tolerance phenotype.

Survival of MRSA infected mice lasted from two to seven days and was considered a complex trait for QTL analysis. For early survival, there was a significant peak on Chromosome 18. The WSB allele at this locus contributed to shorter survival. Seven genes in this region have mutations that have a predicted high impact on protein function. While any of these variants could contribute to the reduced survival phenotype, based on mRNA expression data we collected, we focused on Cadherin2 (*Cdh2*) and NPC intracellular cholesterol transporter 1 (*Npc1*).

Chd2 encodes N-cadherin, which mediates calcium-dependent cell-cell adhesion [114]. In humans, *CDH2* variants are associated with arrhythmogenic right ventricular cardiomyopathy (ARVC) [115, 116]. In mouse models, *Cdh2* conditional knockouts have

abnormal heart structure and function [117]. *S. aureus* manipulates cell-cell adhesion for biofilm formation [118] and changes in the cardiac wall structure to invade tissues [84]. *S. aureus* may use abnormalities in the cardiac wall structure created by the WSB *Cdh2* variants to colonize early in infection.

The primary candidate gene in this QTL, *Npc1*, is present in the membrane of endosomes and lysosomes and mediates intracellular cholesterol trafficking [119]. In humans, mutations in *NPC1* cause Niemann–Pick Type C disease, leading to massive accumulation of cholesterol in lysosomes in all tissues and premature death [120]. Defects in *Npc1* can lead to increased lipid storage in macrophages and a chronic inflammatory condition [121, 122]. NPC1 is also the primary host factor responsible for Ebola, and other filovirus, entry into the cell [123]. These viruses use the *Npc1* receptor in endosomes and lysosomes to trigger a membrane fusion process that allows the expulsion of the viral genome into the cytoplasm and subsequent viral replication [124]. *Npc1* also plays an important role in Human Immunodeficiency virus type-1 (HIV-1) [125], Hepatitis C virus [126] and Chikungunya virus infections [127].

Little is known about the role of *Npc1* in bacterial infections. In a hematopoietic mouse model, *Npc1* mutant mice have a significant increase in the relative abundance of *Staphylococcus* ssp. in their intestine [128], suggesting a role for *Npc1* in keeping *Staphylococcus* ssp. at a low level in this niche. Mutations in *Npc1* impair steady-state autophagosome maturation and interfere with the autophagic trafficking of bacteria to lysosomes in macrophages [129]. *S. aureus* manipulates autophagy in both neutrophils and macrophages to promote its survival and escape [130] [131, 132]. In a large human GWAS study, several SNPs within the *Npc1* gene are associated with changes in

neutrophil counts, linking this gene to neutrophil abundance (n = 173,480) [133]. CC mouse strains carrying the WSB allele of *Npc1* have a missense mutation. This altered form of *Npc1* may interfere with autophagy in macrophages and neutrophils, such that *S. aureus* can survive initial phagocytosis leading to the early susceptibility phenotype.

The A/J allele on Chromosome 18 contributed to reduced survival of MRSA infected mice on day 7. A/J mice are highly susceptible to a different strain of *S. aureus* (SH1000) [26]. Among the 13 protein-coding genes with high impact variants in this region, five matched the founder effect allele pattern. *Ifi44* and *Ifi44l* are our primary candidates at this locus. *Ifi44* has a missense mutation, and *Ifi44l* has a high-impact variant in the gene's promoter region. In mice and humans, *Ifi44l* is a paralog of *Ifi44* and belongs to the Interferon stimulated gene (ISG) family. Both these genes encode proteins with similar size and sequence identity, but it is unclear if they have redundant or distinct functions [134].

Since there was no difference in mRNA expression for *Ifi44* between the founder genotypes, we focused on *Ifi44l*, which was expressed significantly higher in strains with A/J backgrounds. *Ifi44l* promotes macrophage differentiation during bacterial infection and facilitates inflammatory cytokine secretion [135]. Overexpression of *Ifi44* or *Ifi44*L was sufficient to control respiratory syncytial virus (RSV) infection [134]. *Ifi44l* represses the interferon response, protecting the host from the negative effects of the innate immune response during viral infection [136]. The A/J *Ifi44l* allele may be less effective in controlling the interferon response, reducing the survival of *S. aureus* infected mice in the later stages of infection.

Ours is the first study of the effects of host genetic variation during MRSA USA300 sepsis in a genetically diverse inbred mouse panel. A series of previous studies examined the genetic differences that influence *S. aureus* (strain Sanger-476) infection in A/J and BL/6 mice using a chromosome substitution strain (CSS) model [27-29]. Six genes belonging to three different chromosomes (Chr 11 – *Dusp3, Psme3*; Chr 8 – *Crif1, Cd97*; Chr 18 – *Tnfaip8, Seh1l*) were implicated in susceptibility after infection with *S. aureus*. The mechanism of susceptibility in A/J mice was attributed to increased inflammation and a decreased immune response in response to *S. aureus* infection [27].

We did not identify any genes in common with this previous work, likely due to the differences in both the pathogen and the mouse strains used in both studies [27]. Like USA300, Sanger-476 is a community-acquired strain collected in the United Kingdom but is sensitive to methicillin [137]. USA300 also has additional pathogenicity islands, including SaPI5 and SaPIm4, that are absent in the Sanger-476 strain [138]. During infection, USA300 also produces higher amounts of virulence factors compared to other MRSA strains [16, 139, 140]. These genetic differences make USA300 distinct from, and potentially more virulent than, other community-acquired clones of MRSA. On the host side, CC founders include six additional inbred strains (three wild-derived), making the collection of CC strains more genetically diverse than the CSS panel. However, given that studies using the CSS panel identified increased inflammation and defective immune responses as critical to MRSA resistance, we were encouraged to see the mutations in the genes we shortlisted (*Npc1*, *Ifi44l*) also contribute to increase inflammation and a defective immune response.

Using survival, colonization, telemetry, and histology data, we show the diversity underlying the host response to MRSA USA300 infection. We successfully classified CC strains into susceptible, resistant, and tolerant phenotypes with respect to MRSA infection and identified several immune factors that may moderate these phenotypes. We also described MRSA models for studying sex differences, resistance, MRSA mediated heart damage, and pneumonia. We identified pathways, IL-1, and ERK1/2, that could be involved in the mechanisms of tolerance to MRSA infection. Finally, we have described two novel genomic regions that influence early and late survival after MRSA infections. With several *S. aureus* vaccines failing at human clinical trials [141, 142], our data support strong consideration of host genetics as an important factor while designing therapeutics and vaccines against pathogens.

Materials and Methods

Ethics statement

All mouse studies followed the Guide for the Care and Use of Laboratory of Animals of the National Institutes of Health. The animal protocols (2015-0315 D and 2018-0488 D) were reviewed and approved by Texas A&M Institutional Animal Care and Use Committee (IACUC).

Bacterial strains and media

Methicillin-resistant *Staphylococcus aureus* isolate (USA300) used in this study was the kind gift of Dr. Magnus Hook (Texas A&M Institute of Biosciences and Technology, Houston). USA300 is a fully virulent, community-acquired clone of MRSA.

Strains were routinely cultured in Luria-Bertani (LB) broth and plates supplemented with antibiotics when needed at 50 mg/L Kanamycin Sulphate. For murine infections, strains were grown aerobically at 37^0C to a stationary phase in LB broth supplemented with Kanamycin.

Murine strains

Both conventional (C57BL/6J) and Collaborative Cross (CC) mice were used for these experiments. In total, three males and three females belonging to 25 different CC strains and C57BL/6J (156 mice) were used. All mice were initially purchased from UNC's Systems Genetics Core Facility (SGCF). They were bred independently at the Division of Comparative Medicine at Texas A&M University (Table S1). Mice were fed Envigo Teklad Global 19% Protein Extrudent Rodent Diet (2919) or Envigo Teklad Rodent Diet (8604) based on strain need. Mice were provided with cardboard huts, food, and water ad libitum [143].

Placement of telemetry devices

Mice (5-7 weeks old) were anesthetized with an isoflurane vaporizer using the Kent Scientific SomnoSuite Low-flow anesthesia system to implant telemetry devices. A midline abdominal incision was made, and Starr Life Science G2 Emitter devices were sutured to the ventral abdominal wall. The abdominal muscle layer was sutured with 5-0 vicryl, and the skin layer was closed using stainless steel wound clips. Buprenorphine (0.0001 mg/g) was administered intraperitoneally before recovery from anesthesia. Mice were monitored twice daily for surgical complications and humanely euthanized when

needed. Surgical clips were removed on the seventh day, and animals were allowed to recover for one more week.

Health monitoring

After the recovery from surgery, mice were moved to a BSL-2 facility and acclimated for 5-7 days. Individual cages containing implanted mice were placed onto ER4000 receiver platforms and calibrated to receive signals from the implanted telemetry devices. The outputs, body temperature (once per minute) and gross motor activity (summation of movement per minute), were continuously fed to a computer system for visualization (Fig S8 and Fig S9). We manually scored four health parameters twice daily: physical appearance, body conditioning, and provoked and unprovoked behavior. The scoring scale ranged from 0-3, with zero = normal and three = abnormal. Additionally, as a measure of activity, four small nestlets were placed at each corner of the cage in the evening. The following day, the number of nestlets moved from the cage corners into the hut was noted.

Infection with MRSA

After baseline scoring for health, mice (now 8-12 weeks old) were infected with MRSA USA300. Briefly, Mice were anesthetized using isoflurane and infected with 1 x 10^7 CFU in 50 µl of LB broth intravenously at the inferior fornix into the retro-orbital sinus. For each experiment, mice were inoculated at the same time of day. Mice that became moribund dwithin 6 hours of infection were humanely euthanized and removed from the experiment.

Bacterial load determination

After infection, mice were monitored continuously using telemetry readings and twice daily using visual health scoring. Mice that developed illness as measured by telemetry and our health scoring criteria (body condition, physical appearance, provoked and unprovoked behavior) were humanely euthanized by CO2 asphyxiation (Fig S8 and Table S2). After euthanasia, whole blood, serum, and organs (spleen, liver, heart, lung, and kidney) were collected. A consistent region of each organ was collected in 3mL ice-cold PBS and homogenized. The serially diluted homogenate was plated on LB plates supplemented with kanamycin for bacterial enumeration in each organ. Data are expressed as CFU/g of tissue.

Identification of deviation from the circadian pattern of body temperature and activity

A machine-learning algorithm was used to identify the deviation from the circadian pattern of body temperature and activity. Detailed explanation of the methodology and calculations can be found here [48].

Histopathology

After euthanasia, portions of collected organs were fixed in 10% neutral buffered formalin for 24 hours and stored in 70% ethanol. Fixed tissue was embedded in paraffin, sectioned at 5 µm, and stained with hematoxylin and eosin (H&E). A board-certified veterinary pathologist scored all the slides for tissue damage on a scale of 0 to 4 in a blinded manner (Table S3). All the raw pathology data is available in the supplementary file (Table S2). Whole slide images of H&E-stained tissue sections were captured as digital files by scanning at 40X using a 3D Histech Pannoramic SCAN II FL Scanner

(Epredia, MI). Digital files were processed by Aiforia Hub (Cambridge, MA) software to generate images with scaled bars.

Complete blood count

One week before the implantation of telemetry devices, whole blood was collected from each mouse by submandibular bleeding. From the same mice, blood was collected at necropsy after infection by cardiac puncture. Abaxis VetScan HM5, optimized for rodents, was used to analyze blood collected in Ethylene Diamine Tetra Acetic acid (EDTA) tubes. The ratio between the blood parameters after and before infection (value >1 = increased after infection and value < 1 = decreased after infection) was calculated and reported.

Cytokine and chemokine analysis

Serum was separated from the whole blood collected at necropsy. Invitrogen ProcartPlex Cytokine/Chemokine Panel 36 plex kit was used to analyze the serum as per manufacturer instructions. Briefly, magnetic beads were added to each well of the 96-well plate and washed with a wash buffer. 25 ul of serum from each mouse was added in duplicates to the plates along with the standards provided in the kit. After shaking for an hour, 25ul of detection antibody was added to the plates and incubated for 30 minutes. This was followed by adding 50 ul of SAPE for 30 minutes, washing, and 120 ul of reading buffer to each well. The kit screens for the following 36 cytokines and chemokines: IFN gamma; IL-12p70; IL-13; IL-1 beta; IL-2; IL-4; IL-5; IL-6; TNF alpha; GM-CSF; IL-18; IL-10; IL-17A; IL-22; IL-23; IL-27; IL-9; GRO alpha;IP-10; MCP-1; MCP-3; MIP-1 alpha; MIP-1 beta; MIP-2; RANTES; Eotaxin; IFN alpha; IL-15; IL-28; IL-31; IL-

1 alpha; IL-3; G-CSF; LIF; ENA-78/CXCL5; M-CSF. Average values from the duplicates were used for the analysis. To obtain pre-infection levels, serum was collected from age-matched uninfected mice and run using the same protocol mentioned above. The median values of uninfected animals for each strain were used as the baseline for that strain. The difference between infected and uninfected animals (positive value = increased after infection and negative value = decreased after infection) was calculated and reported.

QTL analysis

QTL analysis was performed using R/qtl2 software [53]. This method accounts for the complex population structure in CC strains. Briefly, genome scans were performed on the transformed phenotype and genotypes imputed from the QTL viewer. The generated Logarithm of Odds (LOD) score is the likelihood ratio comparing the hypothesis of a QTL at a given position versus that of no QTL. Each phenotype was randomly shuffled 999 times to establish genome-wide significance, and LOD scores were calculated for each iteration [144]. The 85th percentile of the scores was considered significant for that phenotype. The genomic confidence interval was calculated by dropping the LOD scores by 1.8 for each significant peak. Mouse Genome Informatics (MGI) was used to find the genes and QTL features within each interval [145]. To further shortlist candidate genes, the founder strain distribution pattern was queried against the CC variant database (V3 Version). The Variant effect predictor [VEP] from the ensemble genome database was used to calculate the impact score for the variants [146].

RNA extraction and sequencing

Total RNA was extracted from frozen tissues using Direct-zol RNA Miniprep plus kit following the manufacturer's protocol (Zymo Research - R2073). The purity and quantity of the extracted RNA were analyzed using RNA 6000 Nano LabChip Kit and Bioanalyzer 2100 (Agilent CA, USA, 5067-1511). High-Quality RNA samples with RIN number > 7.0 were used to construct the sequencing library. After total RNA was extracted, mRNA was purified from total RNA (5ug) using Dynabeads Oligo (dT) with two rounds of purification (Thermo Fisher, CA, USA). Following purification, the mRNA was fragmented into short fragments using divalent cations under elevated temperature (Magnesium RNA Fragmentation Module (NEB, cat. e6150, USA) under 94℃ 5-7min). Then the cleaved RNA fragments were reverse-transcribed to create the cDNA by SuperScript™ II Reverse Transcriptase (Invitrogen, cat. 1896649, USA), which were next used to synthesize U-labeled second-stranded DNAs with E. coli DNA polymerase I (NEB, cat.m0209, USA), RNase H (NEB, cat.m0297, USA) and dUTP Solution (Thermo Fisher, cat. R0133, USA). An A-base was then added to the blunt ends of each strand, preparing them for ligation to the indexed adapters. Each adapter contained a T-base overhang for ligating the adapter to the A-tailed fragmented DNA. Dual-index adapters were ligated to the fragments, and size selection was performed with AMPureXP beads. After the heat-labile UDG enzyme (NEB, cat.m0280, USA) treatment of the U-labeled second-stranded DNAs, the ligated products were amplified with PCR by the following conditions: initial denaturation at 95℃ for 3 min; 8 cycles of denaturation at 98℃ for 15 sec, annealing at 60℃ for 15 sec, and extension at 72℃ for 30 sec; and then final extension at 72℃ for 5 min. The average insert size for the final cDNA libraries was 300±50 bp. At last, we performed the 2×150bp paired-end

sequencing (PE150) on an Illumina Novaseq™ 6000 following the vendor's recommended protocol.

RNA sequencing data analysis

Reads were trimmed using trim galore (version 0.6.7) [147-150]. This removed adapters, poly tails, more than 5% of unknown nucleotides, and low-quality reads containing more than 20% of low-quality bases (Q-value <20). Both forward and reverse hard trimmed at 100 base pairs. FastQC was used to verify data quality before and after cleaning [150]. Cleaned reads were aligned and counted against the mouse reference genome (GRCm39) using STAR (version 2.7.9a) aligner [151]. Downstream processing of the data was performed using IDEP 1.0 [152, 153]. Gene counts were analyzed for differentially expressed genes using DESeq2 [154]

Data availability

All of the data points collected on each mouse before and after the infection can be found in the supplementary file (Table S2). Raw RNA sequencing files can be found at SRA (PRJNA1002380).

Acknowledgements

We thank Dr. Magnus Hook for providing the bacterial strain used in this study. We also thank Dr. Karl Broman (University of Wisconsin) for helpful discussions and troubleshooting problems in the rqtl2 google forum. We also would like to thank the members of Helene Andrews-Polymenis Laboratory at Texas A&M University - Dr. Callie Kobayashi, Dr. Joana Rocha, Mrs. Marissa Talamantes, Mr. Chris Bowden, Mr. Connor Mathis, and Mrs. Kaya Mariello for their help in assisting with the experiments.

Figure and Table descriptions

Main Figures

Fig 1: CC strains exhibit a diverse response to MRSA infection. After intravenous infection with MRSA USA300 as described in the Materials and Methods section, we show: A. survival time, B. percent weight change after infection, C. kidney colonization, and D. Total organ colonization; horizontal dotted line represents inoculum dose. CC strains are shown in the ascending order of survival. If survival was equal between two or more strains, strains are arranged in descending order of total organ colonization (the combined colonization of all organs collected). Dots represent individual mice; black dots represent males; green dots represent females. The median and interquartile range are shown for each strain.

Fig 2: Sex differences in survival after MRSA infection. We present pooled data for the four strains that exhibited sex differences in survival: A. survival time, B. percent weight change after infection, C. colonization across organs, and D. pre-infection monocyte and red blood cell counts (U – Uninfected). Each point represents an individual mouse; filled circles represent males; triangles represent females. Each color represents a CC strain as noted in the legend. Medians with 95% confidence interval are shown for each strain. A, B, and D – Student's T-test and C – Mann-Whitney tests were performed to determine statistical significance (* = $P < 0.05$, ** = $P < 0.01$, *** = $P < 0.001$, **** = $P < 0.0001$)

Fig 3: Tissue damage correlates poorly with survival. A stacked bar plot showing the tissue damage score for five organs (Kidney = green, spleen = purple, liver = yellow, heart = blue, lung = orange). Pathology in each tissue was blindly scored by a pathologist on a scale of 0 = no damage, to 4= severe damage.

Fig 4: Several immune parameters differentiate the CC phenotypes. A. Mean neutrophil levels in uninfected mice (S – susceptible, T – Tolerant, R – Resistant). B. Mean change in cytokine and chemokine levels after infection (Purple – Tolerant, Blue – Resistant). C. Top pathways from Gene Ontology (GO) enrichment analysis using differentially expressed genes between tolerant and resistant strains. Lines represent standard error of the mean. Student's T-test was performed to determine statistical significance (* = $P < 0.05$, ** = $P < 0.01$, **** = $P < 0.0001$)

Fig 5. Genomic regions involved in survival after MRSA infection. LOD plots for square root transformed survival phenotype (percentage of animals that survived at the end of each day). A. Early survival (day 2 post-infection) peak on chromosome 18. B. Late survival (day 7 post-infection) peak on chromosome 3. The dotted (Red – 95%, Blue – 90%, Green – 85%) lines represent the significant LOD scores for 999 permutations.

Fig 6. Strongest candidate genes on chromosome 18 for early survival. A. Box plot showing the founder allele contribution at the highest marker on the peak. Each dot represents a strain, lines represent minimum to maximum. B. Genes with high-impact variants shortlisted using the founder effect pattern. C. Mean kidney mRNA expression values after infection (log-transformed). The number of animals is given within brackets.

Lines represent standard error of the mean values. ANOVA with multiple comparison correction using Tukey test was performed (**** = P < 0.0001).

Fig 7. Strongest candidate genes on chromosome 3 for late survival. A. Box plot showing the founder allele contribution at the highest marker on the peak. Each dot represents a strain, lines represent minimum to maximum. B. Genes with high-impact variants shortlisted using the founder effect pattern. C. Mean kidney mRNA expression values after infection (log-transformed). The number of animals sequenced for each founder allele is within the brackets. Lines represent standard error of the mean values. ANOVA with multiple comparison correction using Tukey test was performed (**** = P < 0.0001).

Supplementary Figures

Fig S1: Colonization in other organs. A. Liver colonization. B. spleen colonization, C. heart colonization. D. lung colonization. Strains are shown in ascending order of survival. Where survival was equal, strains are arranged in descending order of total organ colonization. Dots represent individual mice; black dots represent males; green dots represent females. The median and interquartile range are shown for each strain.

Fig S2: Correlation with survival. Heat map showing Spearman correlation 'R' values between survival, weight change, organ colonization, and tissue damage scores.

Fig S3. Representative images of histology scoring scheme. Tissues were sectioned and stained with H&E for scoring. Shows the 400X magnification of representative scoring for all the organs.

Fig S4: Time to deviation from the normal circadian pattern. Plot showing the number of animals that deviated from their normal pattern as identified by telemetry system (machine - dot) vs. Laboratory worker (human - squares)

Fig S5: Differentially expressed genes between tolerant and resistant strains using DEseq2. A. Venn diagram showing the number of up-regulated and down-regulated genes in tolerant strains. B. Tree enrichment analysis using GO terms.

Fig S6. Impact of sex on QTL regions. LOD plots for square root transformed survival phenotype excluding the four sex difference strains. A. Early survival. B. Late survival. The dotted (Red – 99%, Blue – 95%, Green – 90%) lines represent the significant LOD scores for 999 permutations.

Fig S7. QTL plots for other phenotypes. A. LOD plot for rank transformed relative abundance values for significant genera. The dotted lines (Green – 85%, Blue – 90%, Red – 95%) represent significant thresholds. B. Founder effect plot for the significant chromosomes. C. Genotype X Phenotype plot for the highest SNP on the significant chromosome.

Fig S8. Circadian pattern for all mice involved in the study. Blue line represents temperature, black line represents activity and red line represents the time of infection.

Fig S9. Temperature change after infection. Change in temperature for each mouse after infection (for 48 hours). The data is grouped by CC strain and colored lines in each plot represent the strain averages.

Supplementary Tables

Table S1: Mouse strains used in this study. Number of mice, origin, and location of breeding for all the mice used in the study.

Table S2: Data associated with each mouse. All the pre-infection and post-infection data associated with each mouse in the study.

Table S3: Tissue scoring matrix with descriptions. The final score per organ corresponds to the highest score assigned to a single category.

Table S4: Shortlisted variants for survival peaks. Sheet Chr_18 – high impact variants on chromosome 3 for ESMI. Sheet Chr_3 – high impact variants on chromosome 3 for LSMI.

Table S5: QTL regions for other phenotypes. At 85% (Sheet1) and 95 % (Sheet 2%) significance threshold for 999 permutations.

Table S6: Shortlisted variants for other phenotypes. High impact variants in the QTL regions listed on Table S5.

References

1. Lowy, F.D., *Staphylococcus aureus infections.* N Engl J Med, 1998. **339**(8): p. 520-32.
2. Krismer, B., et al., *The commensal lifestyle of Staphylococcus aureus and its interactions with the nasal microbiota.* Nat Rev Microbiol, 2017. **15**(11): p. 675-687.
3. Wertheim, H.F., et al., *The role of nasal carriage in Staphylococcus aureus infections.* The Lancet infectious diseases, 2005. **5**(12): p. 751-762.
4. Laux, C., A. Peschel, and B. Krismer, *Staphylococcus aureus Colonization of the Human Nose and Interaction with Other Microbiome Members.* Microbiol Spectr, 2019. **7**(2).
5. Haag, A.F., J.R. Fitzgerald, and J.R. Penadés, *Staphylococcus aureus in Animals.* Microbiol Spectr, 2019. **7**(3).
6. Tong, S.Y., et al., *Staphylococcus aureus infections: epidemiology, pathophysiology, clinical manifestations, and management.* Clin Microbiol Rev, 2015. **28**(3): p. 603-61.
7. Turner, N.A., et al., *Methicillin-resistant Staphylococcus aureus: an overview of basic and clinical research.* Nat Rev Microbiol, 2019. **17**(4): p. 203-218.
8. Otto, M., *Community-associated MRSA: what makes them special?* Int J Med Microbiol, 2013. **303**(6-7): p. 324-30.
9. Lee, A.S., et al., *Methicillin-resistant Staphylococcus aureus.* Nat Rev Dis Primers, 2018. **4**: p. 18033.
10. Jevons, M.P., A.W. Coe, and M.T. Parker, *Methicillin resistance in staphylococci.* Lancet, 1963. **1**(7287): p. 904-7.
11. Diekema, D.J., et al., *Continued emergence of USA300 methicillin-resistant Staphylococcus aureus in the United States: results from a nationwide surveillance study.* Infect Control Hosp Epidemiol, 2014. **35**(3): p. 285-92.
12. Planet, P.J., *Life After USA300: The Rise and Fall of a Superbug.* J Infect Dis, 2017. **215**(suppl_1): p. S71-S77.
13. Thurlow, L.R., G.S. Joshi, and A.R. Richardson, *Virulence strategies of the dominant USA300 lineage of community-associated methicillin-resistant Staphylococcus aureus (CA-MRSA).* FEMS Immunol Med Microbiol, 2012. **65**(1): p. 5-22.
14. Kempker, R.R., et al., *Association of methicillin-resistant Staphylococcus aureus (MRSA) USA300 genotype with mortality in MRSA bacteremia.* J Infect, 2010. **61**(5): p. 372-81.
15. Kreisel, K.M., et al., *USA300 methicillin-resistant Staphylococcus aureus bacteremia and the risk of severe sepsis: is USA300 methicillin-resistant Staphylococcus aureus associated with more severe infections?* Diagn Microbiol Infect Dis, 2011. **70**(3): p. 285-90.
16. Montgomery, C.P., et al., *Comparison of virulence in community-associated methicillin-resistant Staphylococcus aureus pulsotypes USA300 and USA400 in a rat model of pneumonia.* J Infect Dis, 2008. **198**(4): p. 561-70.
17. Cheung, G.Y., et al., *Role of the accessory gene regulator agr in community-associated methicillin-resistant Staphylococcus aureus pathogenesis.* Infect Immun, 2011. **79**(5): p. 1927-35.

931 18. Li, M., et al., *Evolution of virulence in epidemic community-associated methicillin-*
932 *resistant Staphylococcus aureus.* Proc Natl Acad Sci U S A, 2009. **106**(14): p. 5883-8.
933 19. Shukla, S.K., W. Rose, and S.J. Schrodi, *Complex host genetic susceptibility to*
934 *Staphylococcus aureus infections.* Trends Microbiol, 2015. **23**(9): p. 529-36.
935 20. Kim, H.K., D. Missiakas, and O. Schneewind, *Mouse models for infectious diseases caused*
936 *by Staphylococcus aureus.* J Immunol Methods, 2014. **410**: p. 88-99.
937 21. McAdow, M., et al., *Coagulases as determinants of protective immune responses against*
938 *Staphylococcus aureus.* Infect Immun, 2012. **80**(10): p. 3389-98.
939 22. McAdow, M., et al., *Preventing Staphylococcus aureus sepsis through the inhibition of its*
940 *agglutination in blood.* PLoS Pathog, 2011. **7**(10): p. e1002307.
941 23. Kuklin, N.A., et al., *A novel Staphylococcus aureus vaccine: iron surface determinant B*
942 *induces rapid antibody responses in rhesus macaques and specific increased survival in a*
943 *murine S. aureus sepsis model.* Infect Immun, 2006. **74**(4): p. 2215-23.
944 24. Takeuchi, O., K. Hoshino, and S. Akira, *Cutting Edge: TLR2-Deficient and MyD88-Deficient*
945 *Mice Are Highly Susceptible to Staphylococcus aureus Infection1.* The Journal of
946 Immunology, 2000. **165**(10): p. 5392-5396.
947 25. Deshmukh, H.S., et al., *Critical role of NOD2 in regulating the immune response to*
948 *Staphylococcus aureus.* Infect Immun, 2009. **77**(4): p. 1376-82.
949 26. von Kockritz-Blickwede, M., et al., *Immunological mechanisms underlying the genetic*
950 *predisposition to severe Staphylococcus aureus infection in the mouse model.* Am J
951 Pathol, 2008. **173**(6): p. 1657-68.
952 27. Yan, Q., et al., *Candidate genes on murine chromosome 8 are associated with*
953 *susceptibility to Staphylococcus aureus infection in mice and are involved with*
954 *Staphylococcus aureus septicemia in humans.* PLoS One, 2017. **12**(6): p. e0179033.
955 28. Yan, Q., et al., *Dusp3 and Psme3 are associated with murine susceptibility to*
956 *Staphylococcus aureus infection and human sepsis.* PLoS Pathog, 2014. **10**(6): p.
957 e1004149.
958 29. Ahn, S.H., et al., *Two genes on A/J chromosome 18 are associated with susceptibility to*
959 *Staphylococcus aureus infection by combined microarray and QTL analyses.* PLoS Pathog,
960 2010. **6**(9): p. e1001088.
961 30. Noll, K.E., M.T. Ferris, and M.T. Heise, *The Collaborative Cross: A Systems Genetics*
962 *Resource for Studying Host-Pathogen Interactions.* Cell Host Microbe, 2019. **25**(4): p.
963 484-498.
964 31. Threadgill, D.W., et al., *The collaborative cross: a recombinant inbred mouse population*
965 *for the systems genetic era.* Ilar j, 2011. **52**(1): p. 24-31.
966 32. Churchill, G.A., et al., *The Collaborative Cross, a community resource for the genetic*
967 *analysis of complex traits.* Nature genetics, 2004. **36**(11): p. 1133.
968 33. Srivastava, A., et al., *Genomes of the Mouse Collaborative Cross.* Genetics, 2017. **206**(2):
969 p. 537-556.
970 34. Shorter, J.R., et al., *Whole Genome Sequencing and Progress Toward Full Inbreeding of*
971 *the Mouse Collaborative Cross Population.* G3 Genes|Genomes|Genetics, 2019. **9**(5): p.
972 1303-1311.
973 35. Rasmussen, A.L., et al., *Host genetic diversity enables Ebola hemorrhagic fever*
974 *pathogenesis and resistance.* Science, 2014. **346**(6212): p. 987-991.

975 36. Graham, J.B., et al., *Genetic diversity in the collaborative cross model recapitulates*
976 *human West Nile virus disease outcomes.* MBio, 2015. **6**(3).
977 37. Ferris, M.T., et al., *Modeling host genetic regulation of influenza pathogenesis in the*
978 *collaborative cross.* PLoS Pathog, 2013. **9**(2): p. e1003196.
979 38. Xiong, H., et al., *Genomic profiling of collaborative cross founder mice infected with*
980 *respiratory viruses reveals novel transcripts and infection-related strain-specific gene and*
981 *isoform expression.* G3 (Bethesda), 2014. **4**(8): p. 1429-44.
982 39. Graham, J.B., et al., *Baseline T cell immune phenotypes predict virologic and disease*
983 *control upon SARS-CoV infection in Collaborative Cross mice.* PLoS Pathog, 2021. **17**(1): p.
984 e1009287.
985 40. Brinkmeyer-Langford, C.L., et al., *Host genetic background influences diverse*
986 *neurological responses to viral infection in mice.* Sci Rep, 2017. **7**(1): p. 12194.
987 41. Jensen, I.J., et al., *Novel Mouse Model of Murine Cytomegalovirus-Induced Adaptive NK*
988 *Cells.* Immunohorizons, 2022. **6**(1): p. 8-15.
989 42. Cartwright, H.N., et al., *Genetic diversity of collaborative cross mice enables*
990 *identification of novel rift valley fever virus encephalitis model.* PLoS Pathog, 2022. **18**(7):
991 p. e1010649.
992 43. Smith, C.M., et al., *Tuberculosis Susceptibility and Vaccine Protection Are Independently*
993 *Controlled by Host Genotype.* mBio, 2016. **7**(5).
994 44. Smith, C.M., et al., *Host-pathogen genetic interactions underlie tuberculosis*
995 *susceptibility in genetically diverse mice.* Elife, 2022. **11**.
996 45. Vered, K., et al., *Susceptibility to Klebsiella pneumonaie infection in collaborative cross*
997 *mice is a complex trait controlled by at least three loci acting at different time points.*
998 BMC Genomics, 2014. **15**: p. 865.
999 46. Lorè, N.I., F.A. Iraqi, and A. Bragonzi, *Host genetic diversity influences the severity of*
1000 *Pseudomonas aeruginosa pneumonia in the Collaborative Cross mice.* BMC Genet, 2015.
1001 **16**: p. 106.
1002 47. Rogovskyy, A.S., et al., *The First Immunocompetent Mouse Model of Strictly Human*
1003 *Pathogen, Borrelia recurrentis.* Infect Immun, 2021. **89**(7): p. e0004821.
1004 48. Scoggin, K., et al., *Genetic background influences survival of infections with Salmonella*
1005 *enterica serovar Typhimurium in the Collaborative Cross.* PLoS Genet, 2022. **18**(4): p.
1006 e1010075.
1007 49. Scoggin, K., et al., *Elucidating Mechanisms of Tolerance to Salmonella Typhimurium*
1008 *across Long-Term Infections Using the Collaborative Cross.* mBio, 2022. **13**(4): p.
1009 e0112022.
1010 50. Alugupalli, K.R., et al., *Identification of collaborative cross mouse strains permissive to*
1011 *Salmonella enterica serovar Typhi infection.* Sci Rep, 2023. **13**(1): p. 393.
1012 51. Ali, R.A., et al., *Platelets Mediate Host Defense against Staphylococcus aureus through*
1013 *Direct Bactericidal Activity and by Enhancing Macrophage Activities.* J Immunol, 2017.
1014 **198**(1): p. 344-351.
1015 52. Yun, S.H., et al., *Platelet Activation: The Mechanisms and Potential Biomarkers.* Biomed
1016 Res Int, 2016. **2016**: p. 9060143.
1017 53. Broman, K.W., et al., *R/qtl2: Software for Mapping Quantitative Trait Loci with High-*
1018 *Dimensional Data and Multiparent Populations.* Genetics, 2019. **211**(2): p. 495-502.

1019 54. Vincent, M., et al., *QTLViewer: an interactive webtool for genetic analysis in the*
1020 *Collaborative Cross and Diversity Outbred mouse populations.* G3
1021 Genes|Genomes|Genetics, 2022. **12**(8).
1022 55. Blake, J.A., et al., *Mouse Genome Database (MGD): Knowledgebase for mouse-human*
1023 *comparative biology.* Nucleic Acids Res, 2021. **49**(D1): p. D981-d987.
1024 56. Clarridge, J.E., 3rd, et al., *Impact of strain typing methods on assessment of relationship*
1025 *between paired nares and wound isolates of methicillin-resistant Staphylococcus aureus.*
1026 J Clin Microbiol, 2013. **51**(1): p. 224-31.
1027 57. Howden, B.P., et al., *Staphylococcus aureus host interactions and adaptation.* Nature
1028 Reviews Microbiology, 2023.
1029 58. Cheng, A.G., et al., *Genetic requirements for Staphylococcus aureus abscess formation*
1030 *and persistence in host tissues.* FASEB J, 2009. **23**(10): p. 3393-404.
1031 59. Wong, C.H., et al., *Nucleation of platelets with blood-borne pathogens on Kupffer cells*
1032 *precedes other innate immunity and contributes to bacterial clearance.* Nature
1033 immunology, 2013. **14**(8): p. 785-792.
1034 60. Pollitt, E.J., et al., *Staphylococcus aureus infection dynamics.* PLoS pathogens, 2018.
1035 **14**(6): p. e1007112.
1036 61. Dias, S.P., M.C. Brouwer, and D. van de Beek, *Sex and Gender Differences in Bacterial*
1037 *Infections.* Infect Immun, 2022. **90**(10): p. e0028322.
1038 62. Fish, E.N., *The X-files in immunity: sex-based differences predispose immune responses.*
1039 Nat Rev Immunol, 2008. **8**(9): p. 737-44.
1040 63. Harbarth, S., et al., *Evaluating the probability of previously unknown carriage of MRSA at*
1041 *hospital admission.* The American journal of medicine, 2006. **119**(3): p. 275. e15-275.
1042 e23.
1043 64. Laupland, K.B., et al., *The changing epidemiology of Staphylococcus aureus bloodstream*
1044 *infection: a multinational population-based surveillance study.* Clinical microbiology and
1045 infection, 2013. **19**(5): p. 465-471.
1046 65. Kaasch, A.J., et al., *Staphylococcus aureus bloodstream infection: a pooled analysis of*
1047 *five prospective, observational studies.* Journal of Infection, 2014. **68**(3): p. 242-251.
1048 66. Maclayton, D.O., et al., *Case-control study of the relationship between MRSA bacteremia*
1049 *with a vancomycin MIC of 2 µg/mL and risk factors, costs, and outcomes in inpatients*
1050 *undergoing hemodialysis.* Clinical therapeutics, 2006. **28**(8): p. 1208-1216.
1051 67. Mansur, N., et al., *Does sex affect 30-day mortality in Staphylococcus aureus*
1052 *bacteremia?* Gender medicine, 2012. **9**(6): p. 463-470.
1053 68. Smit, J., et al., *Gender differences in the outcome of community-acquired Staphylococcus*
1054 *aureus bacteraemia: a historical population-based cohort study.* Clinical Microbiology
1055 and Infection, 2017. **23**(1): p. 27-32.
1056 69. Paulsen, J., et al., *Epidemiology and outcome of Staphylococcus aureus bloodstream*
1057 *infection and sepsis in a Norwegian county 1996–2011: an observational study.* BMC
1058 infectious diseases, 2015. **15**(1): p. 1-10.
1059 70. Kubica, M., et al., *A potential new pathway for Staphylococcus aureus dissemination: the*
1060 *silent survival of S. aureus phagocytosed by human monocyte-derived macrophages.*
1061 PloS one, 2008. **3**(1): p. e1409.

1062 71. Pidwill, G.R., et al., *The Role of Macrophages in Staphylococcus aureus Infection.* Front
1063 Immunol, 2020. **11**: p. 620339.
1064 72. Croize, J., et al., *Improved identification of Staphylococcus aureus using a new*
1065 *agglutination test. Results of an international study.* Apmis, 1993. **101**(6): p. 487-91.
1066 73. Wilkerson, M., et al., *Comparison of five agglutination tests for identification of*
1067 *Staphylococcus aureus.* J Clin Microbiol, 1997. **35**(1): p. 148-51.
1068 74. Shin, P.K., et al., *Characteristics of new Staphylococcus aureus-RBC adhesion mechanism*
1069 *independent of fibrinogen and IgG under hydrodynamic shear conditions.* Am J Physiol
1070 Cell Physiol, 2005. **289**(3): p. C727-34.
1071 75. Gianquinto, E., et al., *Interaction of human hemoglobin and semi-hemoglobins with the*
1072 *Staphylococcus aureus hemophore IsdB: a kinetic and mechanistic insight.* Scientific
1073 Reports, 2019. **9**(1): p. 18629.
1074 76. Spaan, A.N., et al., *Staphylococcus aureus Targets the Duffy Antigen Receptor for*
1075 *Chemokines (DARC) to Lyse Erythrocytes.* Cell Host Microbe, 2015. **18**(3): p. 363-70.
1076 77. Skaar, E.P., et al., *Iron-source preference of Staphylococcus aureus infections.* Science,
1077 2004. **305**(5690): p. 1626-8.
1078 78. Bundgaard, H., et al., *Long-term outcomes of partial oral treatment of endocarditis.* N
1079 Engl J Med, 2019. **10**.
1080 79. Iversen, K., et al., *Partial oral versus intravenous antibiotic treatment of endocarditis.*
1081 New England Journal of Medicine, 2019. **380**(5): p. 415-424.
1082 80. Parker, D., *Humanized Mouse Models of Staphylococcus aureus Infection.* Front Immunol,
1083 2017. **8**: p. 512.
1084 81. Bor, D.H., et al., *Infective Endocarditis in the U.S., 1998–2009: A Nationwide Study.* PLOS
1085 ONE, 2013. **8**(3): p. e60033.
1086 82. Federspiel, J.J., et al., *Increasing US rates of endocarditis with Staphylococcus aureus:*
1087 *1999-2008.* Archives of internal medicine, 2012. **172**(4): p. 363-365.
1088 83. Gibson, G.W., et al., *Development of a mouse model of induced Staphylococcus aureus*
1089 *infective endocarditis.* Comparative medicine, 2007. **57**(6): p. 563-569.
1090 84. Liesenborghs, L., et al., *Staphylococcus aureus endocarditis: distinct mechanisms of*
1091 *bacterial adhesion to damaged and inflamed heart valves.* Eur Heart J, 2019. **40**(39): p.
1092 3248-3259.
1093 85. Wasi, F. and J. Shuter, *Primary bacterial infection of the myocardium.* Front Biosci, 2003.
1094 **8**: p. s228-31.
1095 86. LeLeiko, R.M., D.J. Bower, and C.P. Larsen, *MRSA-associated bacterial myocarditis*
1096 *causing ruptured ventricle and tamponade.* Cardiology, 2008. **111**(3): p. 188-90.
1097 87. Jariwala, P., et al., *Myocardial abscess secondary to staphylococcal septicemia: diagnosis*
1098 *with 3D echocardiography.* Indian Heart J, 2013. **65**(1): p. 124-5.
1099 88. Lee, L.-N., et al., *Characteristics and local risk factors of community-acquired and health-*
1100 *care-associated Staphylococcus aureus pneumonia.* Scientific Reports, 2022. **12**(1): p.
1101 18670.
1102 89. Dell'Isola, G.B., et al., *Noncontact Body Temperature Measurement: Uncertainty*
1103 *Evaluation and Screening Decision Rule to Prevent the Spread of COVID-19.* Sensors
1104 (Basel), 2021. **21**(2).

1105 90. Lippi, G., et al., *Is body temperature mass screening a reliable and safe option for*
1106 *preventing COVID-19 spread?* Diagnosis (Berl), 2021. **9**(2): p. 195-198.
1107 91. Dzien, C., et al., *Covid-19 screening: are forehead temperature measurements during*
1108 *cold outdoor temperatures really helpful?* Wien Klin Wochenschr, 2021. **133**(7-8): p. 331-
1109 335.
1110 92. Sharif Nia, H., et al., *Clinical accuracy and agreement between tympanic and forehead*
1111 *body temperature measurements for screening of patients with COVID-19.* J Clin Nurs,
1112 2022. **31**(21-22): p. 3272-3285.
1113 93. Ngcobo, S., et al., *Pre-infection plasma cytokines and chemokines as predictors of HIV*
1114 *disease progression.* Sci Rep, 2022. **12**(1): p. 2437.
1115 94. Spaan, A.N., et al., *Neutrophils versus Staphylococcus aureus: a biological tug of war.*
1116 Annu Rev Microbiol, 2013. **67**: p. 629-50.
1117 95. Bouma, G., et al., *Recent advances in the understanding of genetic defects of neutrophil*
1118 *number and function.* Br J Haematol, 2010. **151**(4): p. 312-26.
1119 96. Andrews, T. and K.E. Sullivan, *Infections in patients with inherited defects in phagocytic*
1120 *function.* Clin Microbiol Rev, 2003. **16**(4): p. 597-621.
1121 97. Lakshman, R. and A. Finn, *Neutrophil disorders and their management.* J Clin Pathol,
1122 2001. **54**(1): p. 7-19.
1123 98. Pollitt, E.J.G., et al., *Staphylococcus aureus infection dynamics.* PLoS Pathog, 2018. **14**(6):
1124 p. e1007112.
1125 99. Rigby, K.M. and F.R. DeLeo, *Neutrophils in innate host defense against Staphylococcus*
1126 *aureus infections.* Seminars in Immunopathology, 2012. **34**(2): p. 237-259.
1127 100. Hamilton, J.A., *GM-CSF in inflammation.* Journal of Experimental Medicine, 2019. **217**(1).
1128 101. Ali, A., et al., *IL-1 Receptor Antagonist Treatment Aggravates Staphylococcal Septic*
1129 *Arthritis and Sepsis in Mice.* PLoS One, 2015. **10**(7): p. e0131645.
1130 102. Miller, L.S., et al., *MyD88 mediates neutrophil recruitment initiated by IL-1R but not TLR2*
1131 *activation in immunity against Staphylococcus aureus.* Immunity, 2006. **24**(1): p. 79-91.
1132 103. Cohen, T.S. and A.S. Prince, *Bacterial pathogens activate a common inflammatory*
1133 *pathway through IFNλ regulation of PDCD4.* PLoS pathogens, 2013. **9**(10): p. e1003682.
1134 104. Henningsson, L., et al., *Interleukin 15 Mediates Joint Destruction in Staphylococcus*
1135 *Aureus Arthritis.* The Journal of Infectious Diseases, 2012. **206**(5): p. 687-696.
1136 105. van Drongelen, V., et al., *Reduced filaggrin expression is accompanied by increased*
1137 *Staphylococcus aureus colonization of epidermal skin models.* Clin Exp Allergy, 2014.
1138 **44**(12): p. 1515-24.
1139 106. Boisson, B., *The genetic basis of pneumococcal and staphylococcal infections: inborn*
1140 *errors of human TLR and IL-1R immunity.* Human Genetics, 2020. **139**(6): p. 981-991.
1141 107. Krishna, S. and L.S. Miller, *Innate and adaptive immune responses against*
1142 *Staphylococcus aureus skin infections.* Seminars in Immunopathology, 2012. **34**(2): p.
1143 261-280.
1144 108. Hultgren, O.H., L. Svensson, and A. Tarkowski, *Critical role of signaling through IL-1*
1145 *receptor for development of arthritis and sepsis during Staphylococcus aureus infection.* J
1146 Immunol, 2002. **168**(10): p. 5207-12.
1147 109. Wortzel, I. and R. Seger, *The ERK Cascade: Distinct Functions within Various Subcellular*
1148 *Organelles.* Genes Cancer, 2011. **2**(3): p. 195-209.

1149 110. von Kriegsheim, A., et al., *Cell fate decisions are specified by the dynamic ERK*
1150 *interactome.* Nat Cell Biol, 2009. **11**(12): p. 1458-64.
1151 111. Lucas, R.M., L. Luo, and J.L. Stow, *ERK1/2 in immune signalling.* Biochem Soc Trans, 2022.
1152 **50**(5): p. 1341-1352.
1153 112. Kopczynski, M., et al., *Selective Extracellular Signal-Regulated Kinase 1/2 (ERK1/2)*
1154 *Inhibition by the SCH772984 Compound Attenuates In Vitro and In Vivo Inflammatory*
1155 *Responses and Prolongs Survival in Murine Sepsis Models.* Int J Mol Sci, 2021. **22**(19).
1156 113. Zhao, S., et al., *TGF-β1 promotes Staphylococcus aureus adhesion to and invasion into*
1157 *bovine mammary fibroblasts via the ERK pathway.* Microb Pathog, 2017. **106**: p. 25-29.
1158 114. Chen, Y., et al., *Identification of a novel variant in N-cadherin associated with dilated*
1159 *cardiomyopathy.* Front Med (Lausanne), 2022. **9**: p. 944950.
1160 115. Mayosi, B.M., et al., *Identification of Cadherin 2 (CDH2) Mutations in Arrhythmogenic*
1161 *Right Ventricular Cardiomyopathy.* Circ Cardiovasc Genet, 2017. **10**(2).
1162 116. Ye, J.Z., et al., *Reevaluation of genetic variants previously associated with*
1163 *arrhythmogenic right ventricular cardiomyopathy integrating population-based cohorts*
1164 *and proteomics data.* Clin Genet, 2019. **96**(6): p. 506-514.
1165 117. Kostetskii, I., et al., *Induced deletion of the N-cadherin gene in the heart leads to*
1166 *dissolution of the intercalated disc structure.* Circ Res, 2005. **96**(3): p. 346-54.
1167 118. Herman-Bausier, P., et al., *Staphylococcus aureus Fibronectin-Binding Protein A Mediates*
1168 *Cell-Cell Adhesion through Low-Affinity Homophilic Bonds.* mBio, 2015. **6**(3): p. e00413-
1169 15.
1170 119. Pfeffer, S.R., *NPC intracellular cholesterol transporter 1 (NPC1)-mediated cholesterol*
1171 *export from lysosomes.* J Biol Chem, 2019. **294**(5): p. 1706-1709.
1172 120. Pentchev, P.G., *Niemann–Pick C research from mouse to gene.* Biochimica et Biophysica
1173 Acta (BBA) - Molecular and Cell Biology of Lipids, 2004. **1685**(1): p. 3-7.
1174 121. Hendrikx, T., et al., *Lysosomal cholesterol accumulation: driver on the road to*
1175 *inflammation during atherosclerosis and non-alcoholic steatohepatitis.* Obes Rev, 2014.
1176 **15**(5): p. 424-33.
1177 122. Xu, X., et al., *Lysosomal cholesterol accumulation in macrophages leading to coronary*
1178 *atherosclerosis in CD38(-/-) mice.* J Cell Mol Med, 2016. **20**(6): p. 1001-13.
1179 123. Carette, J.E., et al., *Ebola virus entry requires the cholesterol transporter Niemann–Pick*
1180 *C1.* Nature, 2011. **477**(7364): p. 340-343.
1181 124. Morales-Tenorio, M., et al., *Potential pharmacological strategies targeting the Niemann-*
1182 *Pick C1 receptor and Ebola virus glycoprotein interaction.* European Journal of Medicinal
1183 Chemistry, 2021. **223**: p. 113654.
1184 125. Tang, Y., et al., *Deficiency of niemann-pick type C-1 protein impairs release of human*
1185 *immunodeficiency virus type 1 and results in Gag accumulation in late*
1186 *endosomal/lysosomal compartments.* Journal of virology, 2009. **83**(16): p. 7982-7995.
1187 126. Sainz, B., et al., *Identification of the Niemann-Pick C1–like 1 cholesterol absorption*
1188 *receptor as a new hepatitis C virus entry factor.* Nature Medicine, 2012. **18**(2): p. 281-
1189 285.
1190 127. Wichit, S., et al., *Imipramine Inhibits Chikungunya Virus Replication in Human Skin*
1191 *Fibroblasts through Interference with Intracellular Cholesterol Trafficking.* Sci Rep, 2017.
1192 **7**(1): p. 3145.

1193 128. Houben, T., et al., *Hematopoietic Npc1 mutation shifts gut microbiota composition in*
1194 *Ldlr(-/-) mice on a high-fat, high-cholesterol diet.* Sci Rep, 2019. **9**(1): p. 14956.
1195 129. Schwerd, T., et al., *Impaired antibacterial autophagy links granulomatous intestinal*
1196 *inflammation in Niemann-Pick disease type C1 and XIAP deficiency with NOD2 variants*
1197 *in Crohn's disease.* Gut, 2017. **66**(6): p. 1060-1073.
1198 130. Prajsnar, T.K., et al., *The autophagic response to Staphylococcus aureus provides an*
1199 *intracellular niche in neutrophils.* Autophagy, 2021. **17**(4): p. 888-902.
1200 131. Dai, Y., et al., *Heterogeneous Vancomycin-Intermediate Staphylococcus aureus Uses the*
1201 *VraSR Regulatory System to Modulate Autophagy for Increased Intracellular Survival in*
1202 *Macrophage-Like Cell Line RAW264.7.* Front Microbiol, 2019. **10**: p. 1222.
1203 132. O'Keeffe, K.M., et al., *Manipulation of Autophagy in Phagocytes Facilitates*
1204 *Staphylococcus aureus Bloodstream Infection.* Infect Immun, 2015. **83**(9): p. 3445-57.
1205 133. Astle, W.J., et al., *The Allelic Landscape of Human Blood Cell Trait Variation and Links to*
1206 *Common Complex Disease.* Cell, 2016. **167**(5): p. 1415-1429.e19.
1207 134. Busse, D.C., et al., *Interferon-Induced Protein 44 and Interferon-Induced Protein 44-Like*
1208 *Restrict Replication of Respiratory Syncytial Virus.* J Virol, 2020. **94**(18).
1209 135. Jiang, H., et al., *IFI44L as a Forward Regulator Enhancing Host Antituberculosis*
1210 *Responses.* J Immunol Res, 2021. **2021**: p. 5599408.
1211 136. DeDiego, M.L., L. Martinez-Sobrido, and D.J. Topham, *Novel Functions of IFI44L as a*
1212 *Feedback Regulator of Host Antiviral Responses.* J Virol, 2019. **93**(21).
1213 137. Holden, M.T., et al., *Complete genomes of two clinical Staphylococcus aureus strains:*
1214 *evidence for the rapid evolution of virulence and drug resistance.* Proc Natl Acad Sci U S
1215 A, 2004. **101**(26): p. 9786-91.
1216 138. Highlander, S.K., et al., *Subtle genetic changes enhance virulence of methicillin resistant*
1217 *and sensitive Staphylococcus aureus.* BMC Microbiol, 2007. **7**: p. 99.
1218 139. Lee, H.S., et al., *Comparative Study of the Difference in Behavior of the Accessory Gene*
1219 *Regulator (Agr) in USA300 and USA400 Community-Associated Methicillin-Resistant*
1220 *Staphylococcus aureus (CA-MRSA).* J Microbiol Biotechnol, 2021. **31**(8): p. 1060-1068.
1221 140. Jones, M.B., et al., *Genomic and transcriptomic differences in community acquired*
1222 *methicillin resistant Staphylococcus aureus USA300 and USA400 strains.* BMC Genomics,
1223 2014. **15**: p. 1145.
1224 141. Redi, D., et al., *Staphylococcus aureus vaccine preclinical and clinical development:*
1225 *current state of the art.* New Microbiol, 2018. **41**(3): p. 208-213.
1226 142. Miller, L.S., et al., *Development of a vaccine against Staphylococcus aureus invasive*
1227 *infections: Evidence based on human immunity, genetics and bacterial evasion*
1228 *mechanisms.* FEMS Microbiol Rev, 2020. **44**(1): p. 123-153.
1229 143. Nagarajan, A., et al., *Using the collaborative cross to identify the role of host genetics in*
1230 *defining the murine gut microbiome.* Microbiome, 2023. **11**(1): p. 149.
1231 144. Churchill, G.A. and R.W. Doerge, *Empirical threshold values for quantitative trait*
1232 *mapping.* Genetics, 1994. **138**(3): p. 963-71.
1233 145. Bogue, M.A., et al., *Mouse Phenome Database: towards a more FAIR-compliant and*
1234 *TRUST-worthy data repository and tool suite for phenotypes and genotypes.* Nucleic
1235 Acids Res, 2023. **51**(D1): p. D1067-d1074.
1236 146. Cunningham, F., et al., *Ensembl 2022.* Nucleic Acids Res, 2022. **50**(D1): p. D988-d995.

1237 147. Krueger, F., *Taking appropriate QC measures for RRBS-type or other -Seq applications*
1238 *with Trim Galore!* Github, 2019.
1239 148. Kechin, A., et al., *cutPrimers: A New Tool for Accurate Cutting of Primers from Reads of*
1240 *Targeted Next Generation Sequencing.* J Comput Biol, 2017. **24**(11): p. 1138-1143.
1241 149. *FastQC*. 2015.
1242 150. Andrews, S., *FastQC: a quality control tool for high throughput sequence data*. 2010,
1243 Babraham Bioinformatics, Babraham Institute, Cambridge, United Kingdom.
1244 151. Dobin, A., et al., *STAR: ultrafast universal RNA-seq aligner.* Bioinformatics, 2013. **29**(1): p.
1245 15-21.
1246 152. Ge, S.X., E.W. Son, and R. Yao, *iDEP: an integrated web application for differential*
1247 *expression and pathway analysis of RNA-Seq data.* BMC Bioinformatics, 2018. **19**(1): p.
1248 534.
1249 153. Ge, X., *iDEP Web Application for RNA-Seq Data Analysis.* Methods Mol Biol, 2021. **2284**:
1250 p. 417-443.
1251 154. Love, M.I., W. Huber, and S. Anders, *Moderated estimation of fold change and dispersion*
1252 *for RNA-seq data with DESeq2.* Genome Biol, 2014. **15**(12): p. 550.

1253

Fig 1

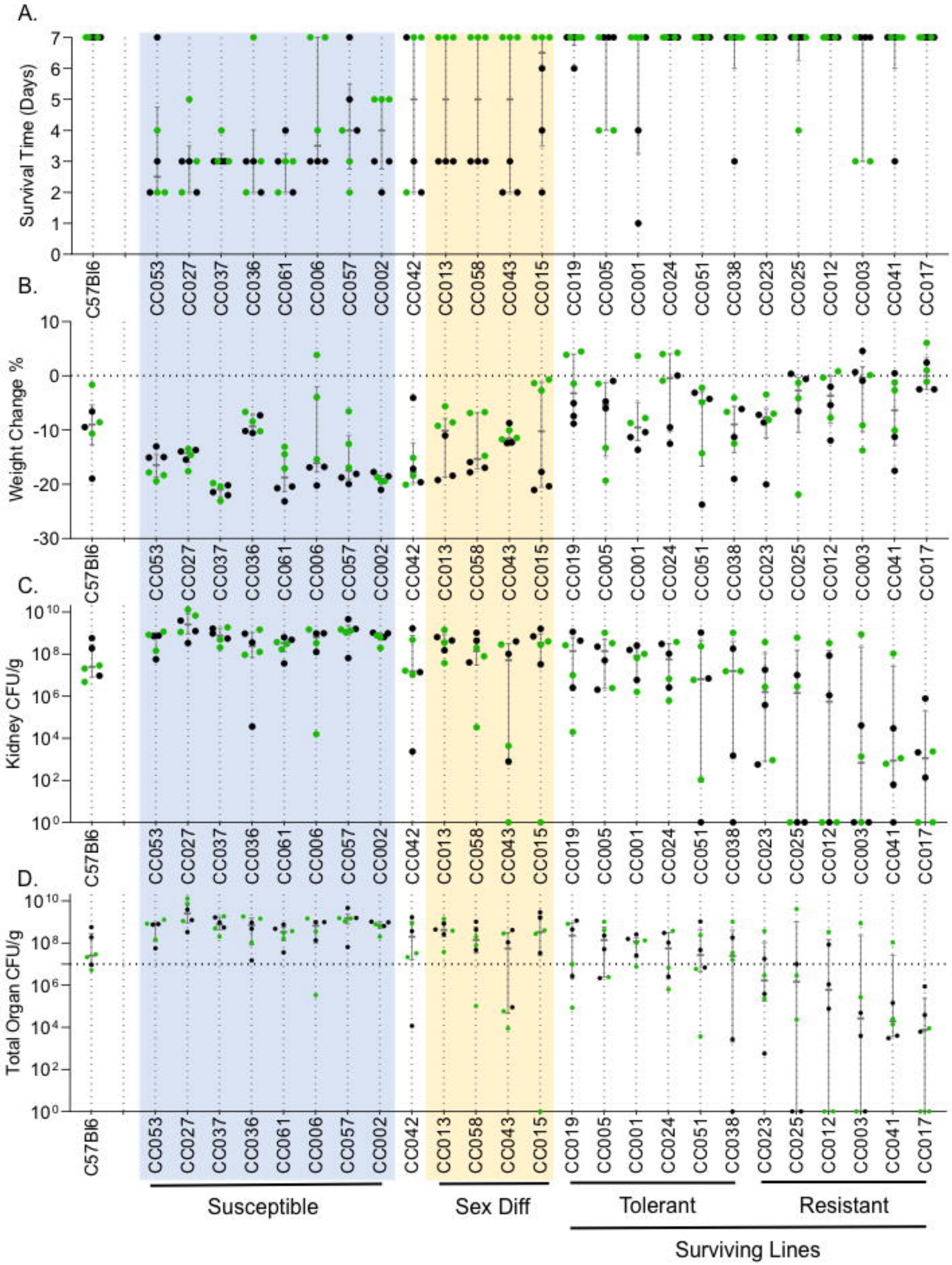
A.
Survival Time (Days)
B.
Weight Change %
C.
Kidney CFU/g
D.
Total Organ CFU/g
C57Bl6
CC053
CC027
CC037
CC036
CC061
CC006
CC057
CC002
CC042
CC013
CC058
CC043
CC015
CC019
CC005
CC001
CC024
CC051
CC038
CC023
CC025
CC012
CC003
CC041
CC017
Susceptible
Sex Diff
Tolerant
Resistant
Surviving Lines

Fig 2

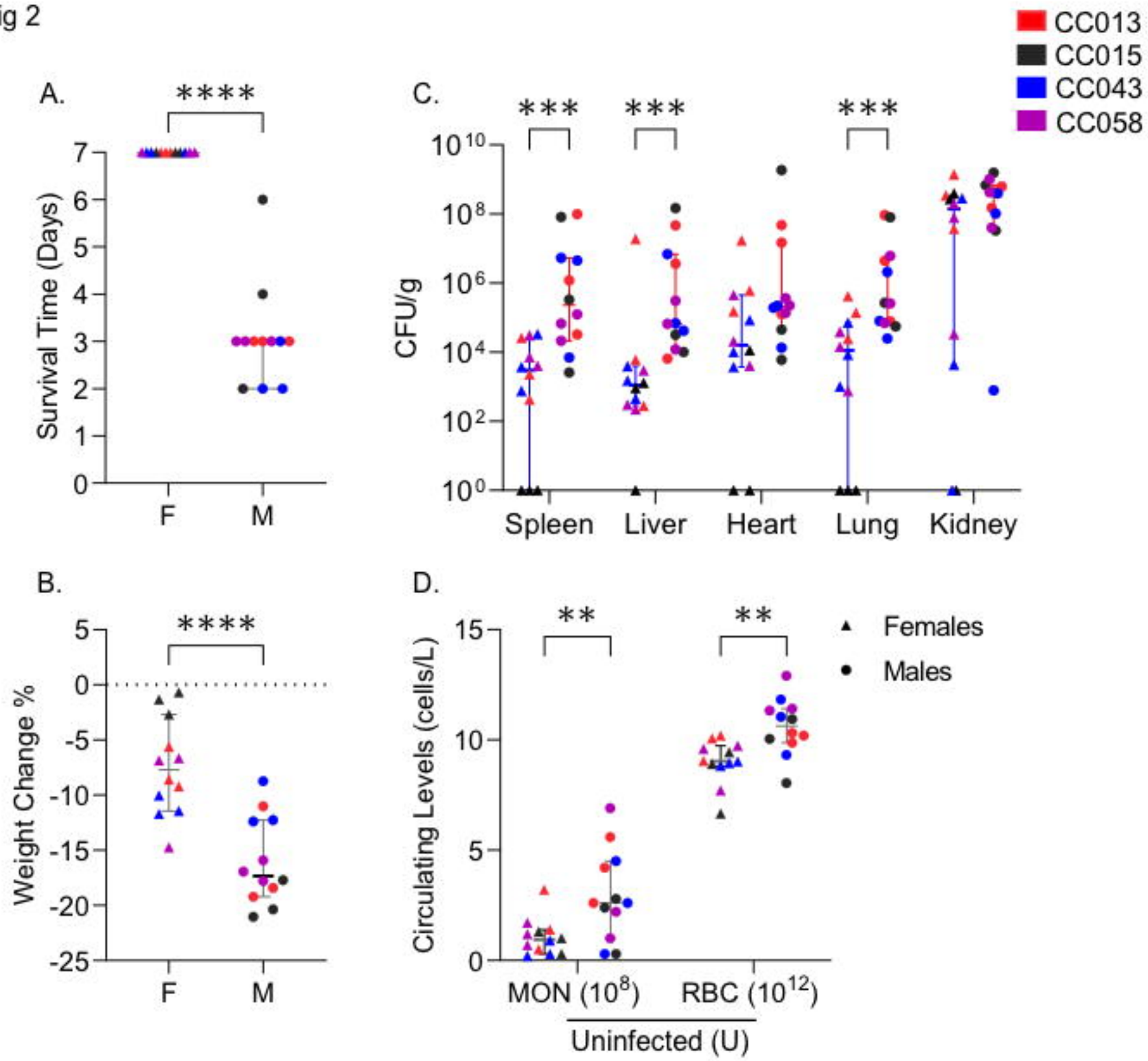
CC013
CC015
CC043
CC058
A.
****
Survival Time (Days)
0
1
2
3
4
5
6
7
F
M
C.
***
***
***
CFU/g
10^{10}
10^{8}
10^{6}
10^{4}
10^{2}
10^{0}
Spleen
Liver
Heart
Lung
Kidney
B.
****
Weight Change %
5
0
-5
-10
-15
-20
-25
F
M
D.
**
**
Circulating Levels (cells/L)
15
10
5
0
Females
Males
MON (10^{8})
RBC (10^{12})
Uninfected (U)

Fig 3

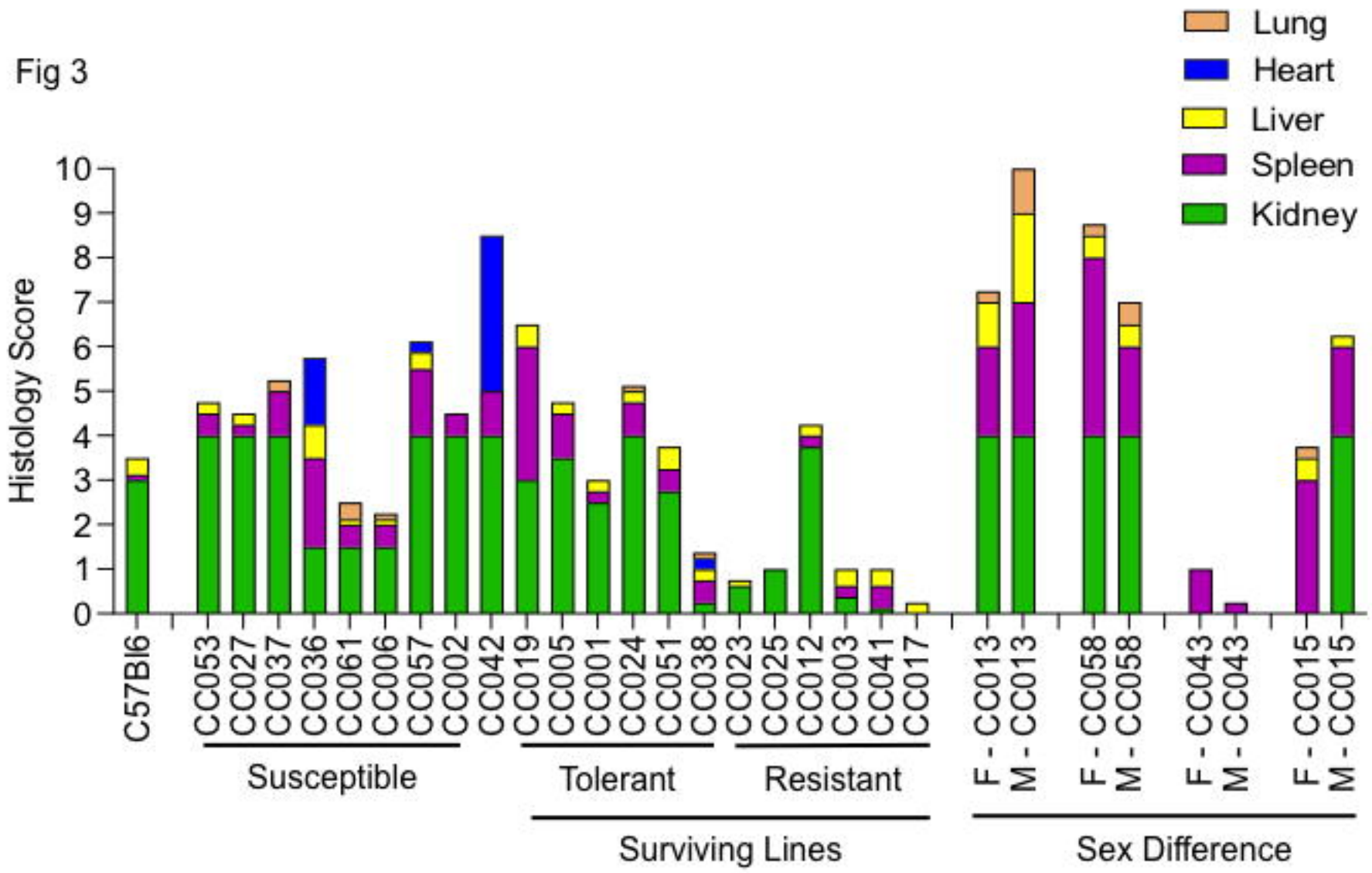
Lung
Heart
Liver
Spleen
Kidney
Histology Score
0
1
2
3
4
5
6
7
8
9
10
C57Bl6
CC053
CC027
CC037
CC036
CC061
CC006
CC057
CC002
CC042
CC019
CC005
CC001
CC024
CC051
CC038
CC023
CC025
CC012
CC003
CC041
CC017
F - CC013
M - CC013
F - CC058
M - CC058
F - CC043
M - CC043
F - CC015
M - CC015
Susceptible
Tolerant
Resistant
Surviving Lines
Sex Difference

Fig 4

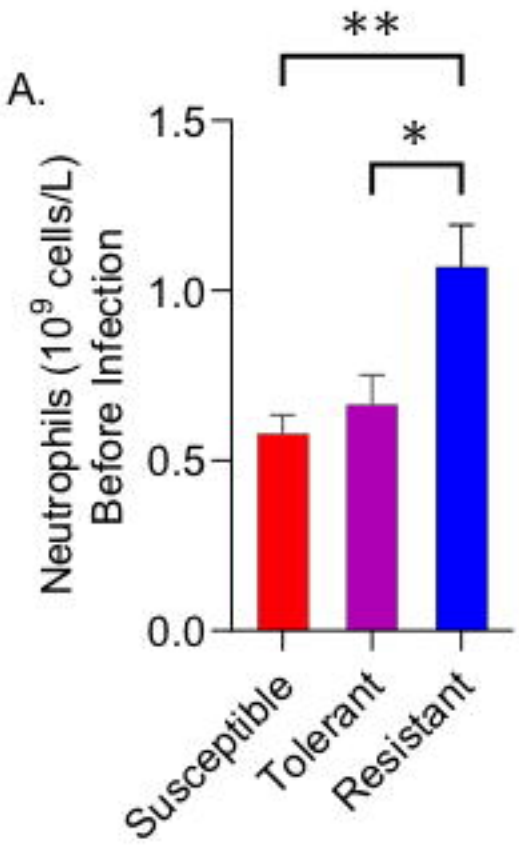
A.
**
*
Neutrophils (10^9 cells/L)
Before Infection
1.5
1.0
0.5
0.0
Susceptible
Tolerant
Resistant

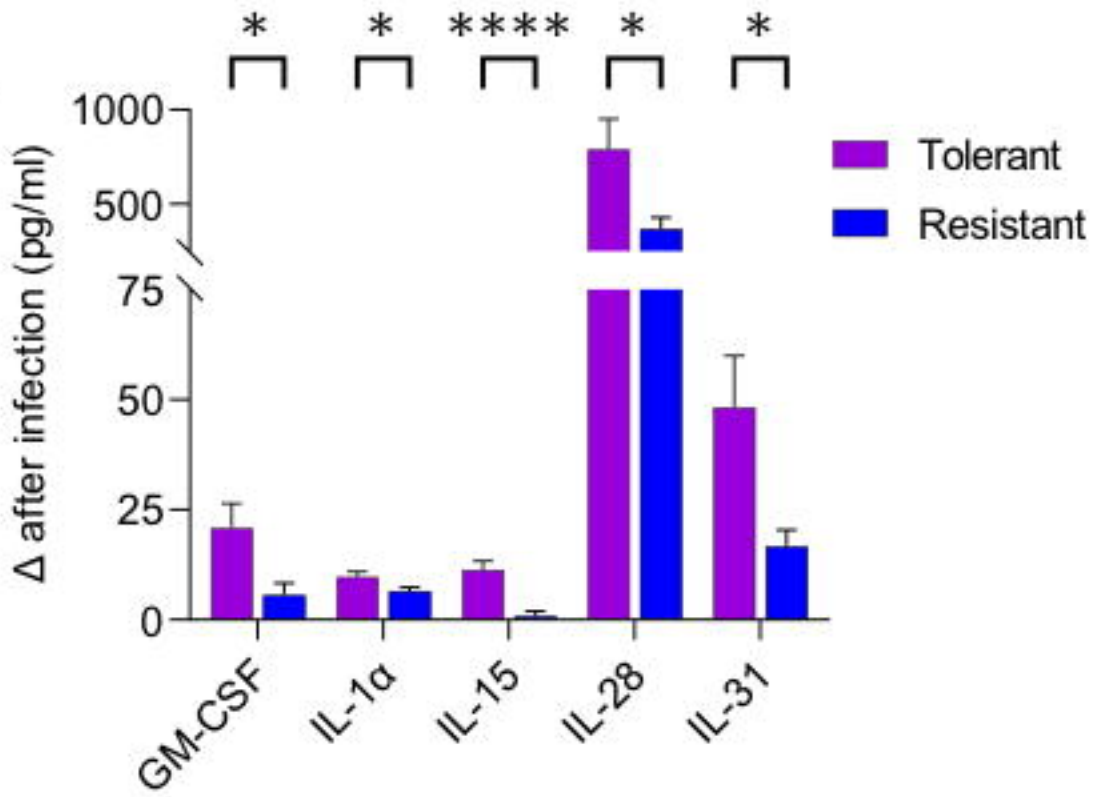
B.
*
*
****
*
*
Δ after infection (pg/ml)
1000
500
75
50
25
0
Tolerant
Resistant
GM-CSF
IL-1α
IL-15
IL-28
IL-31

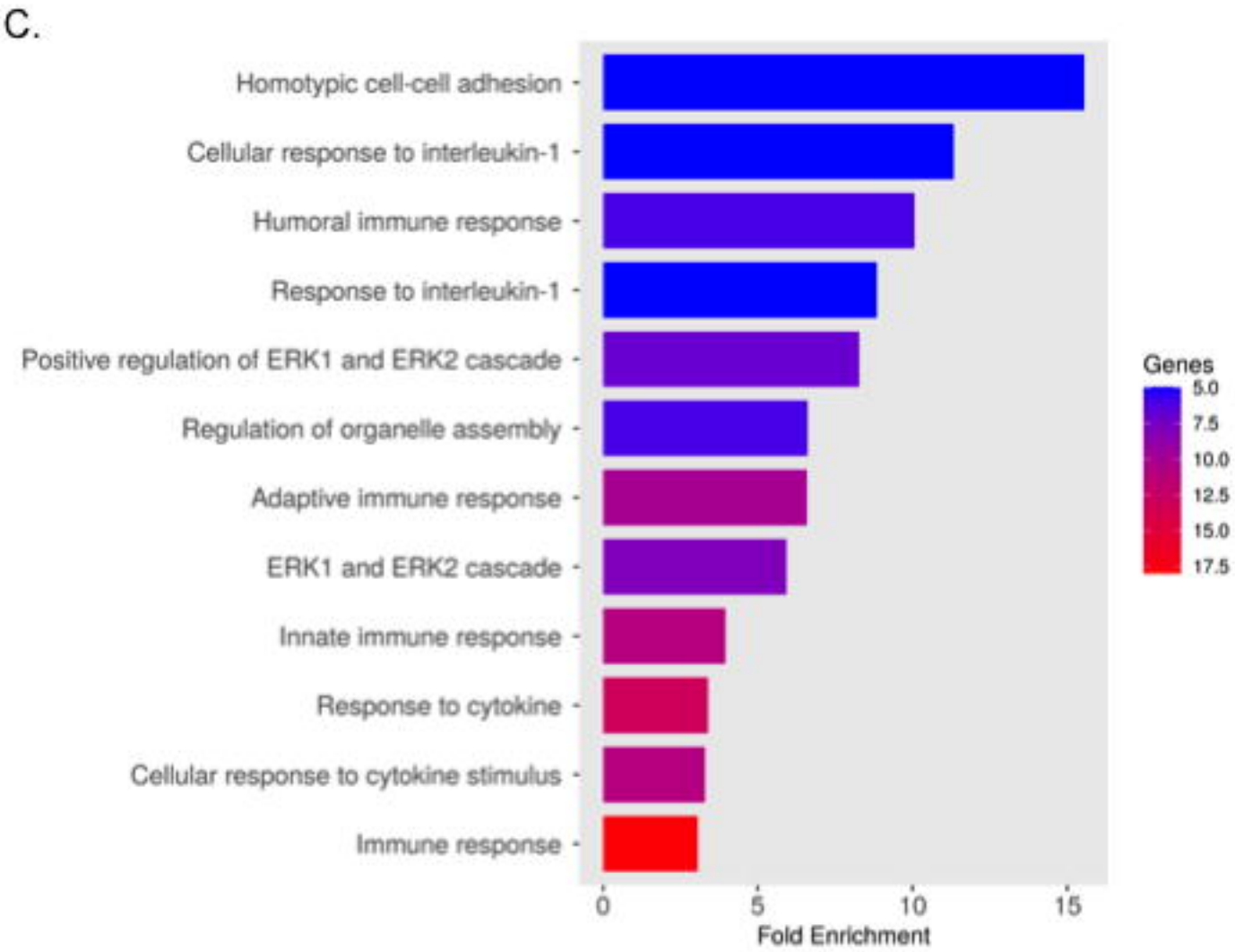
C.
Homotypic cell-cell adhesion
Cellular response to interleukin-1
Humoral immune response
Response to interleukin-1
Positive regulation of ERK1 and ERK2 cascade
Regulation of organelle assembly
Adaptive immune response
ERK1 and ERK2 cascade
Innate immune response
Response to cytokine
Cellular response to cytokine stimulus
Immune response
0
5
10
15
Fold Enrichment
Genes
5.0
7.5
10.0
12.5
15.0
17.5

Fig 5

A.

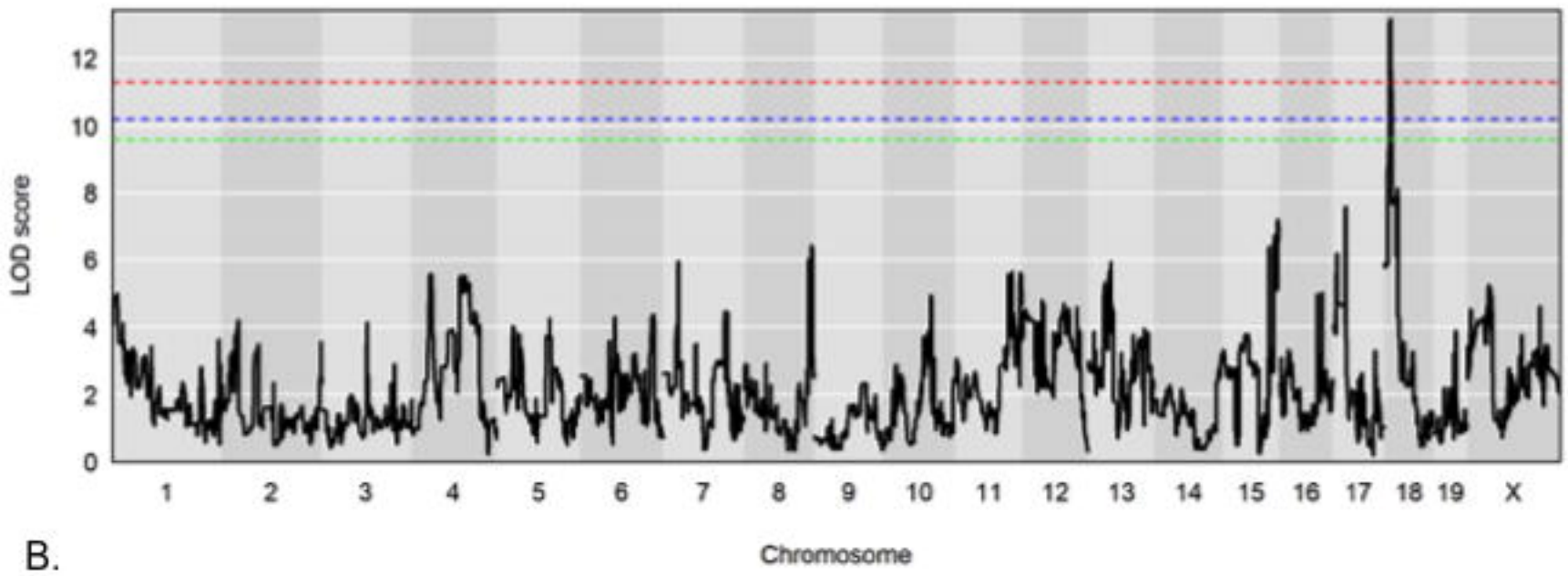
LOD score
0
2
4
6
8
10
12
1 2 3 4 5 6 7 8 9 10 11 12 13 14 15 16 17 18 19 X
Chromosome

B.

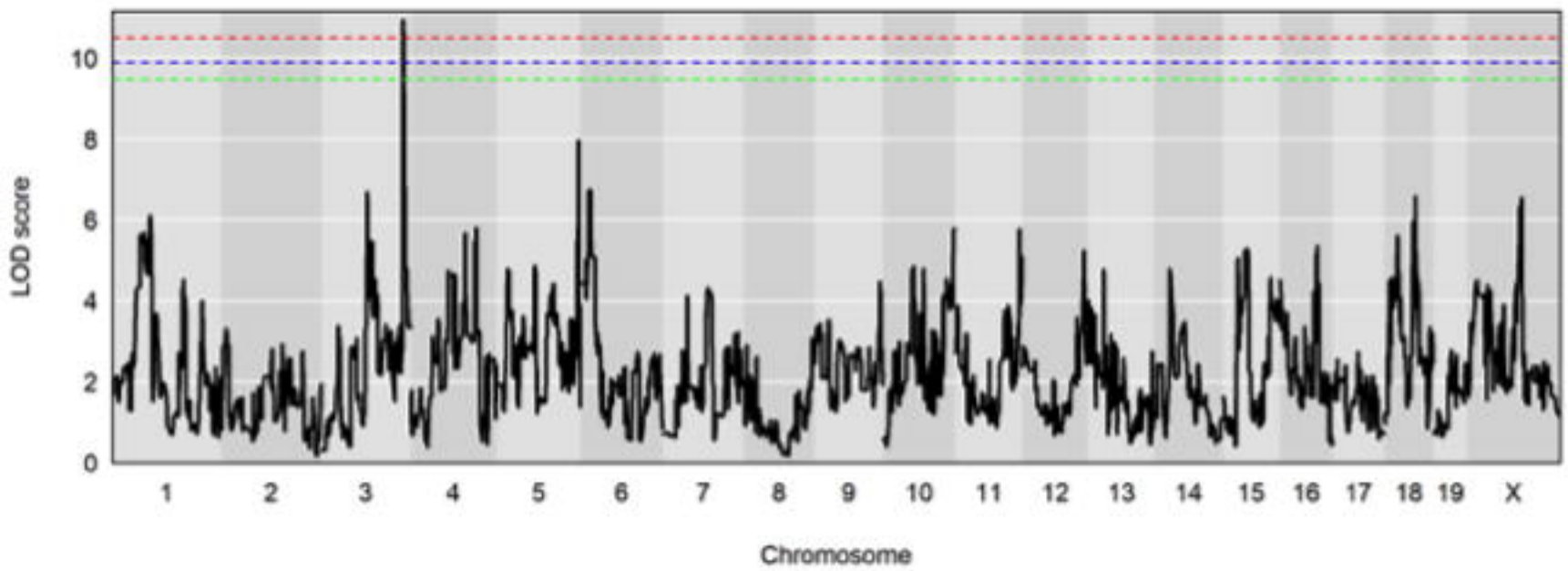
LOD score
0
2
4
6
8
10
1 2 3 4 5 6 7 8 9 10 11 12 13 14 15 16 17 18 19 X
Chromosome

Fig 6

A.

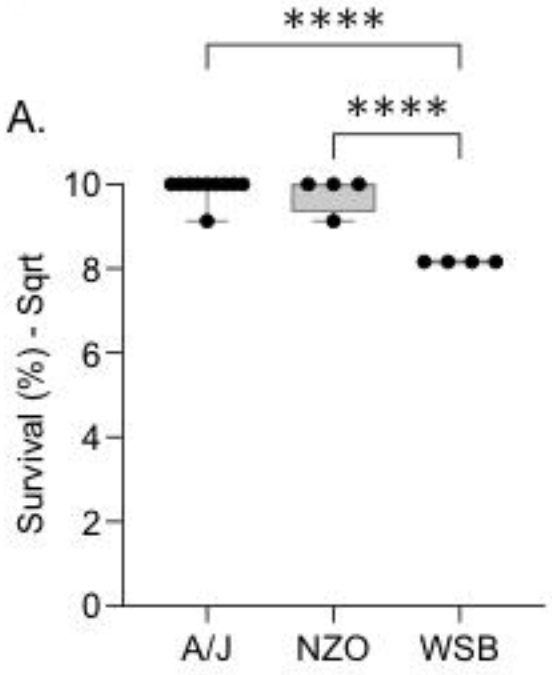

B.

GENE	SNP_ID	A/J	NZO	WSB	Cons
Npc1	rs30985329	A	A	T	missense
Lama3	rs51262081	C	C	G	missense
Cabyr	rs49718484	A	A	G	missense
Osbpl1a	rs48171054	T	T	C	missense
Psma8	rs31135735	A	A	G	missense
Kctd1	rs226935597	G	G	T	missense
Cdh2	rs243156099	C	C	T	splice region

C.

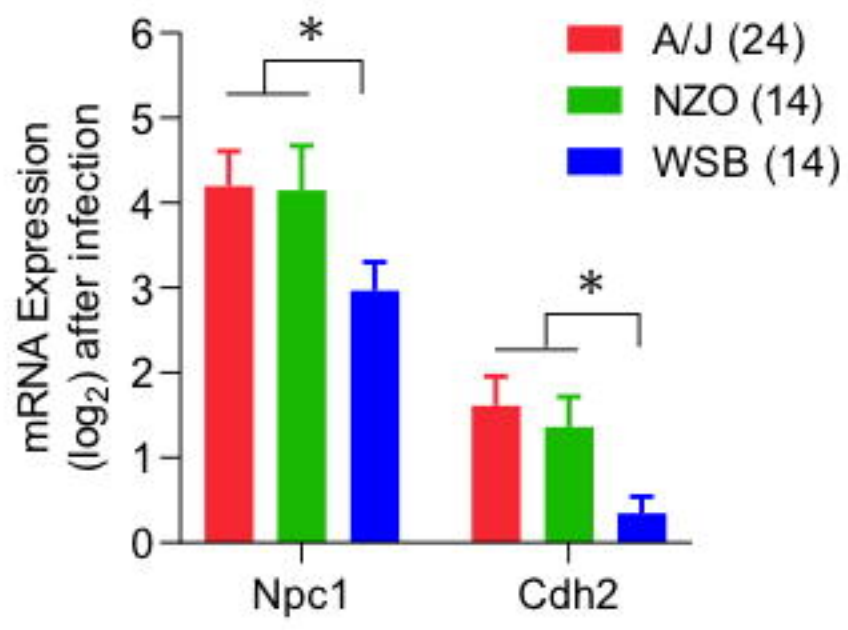

Fig 7

A.

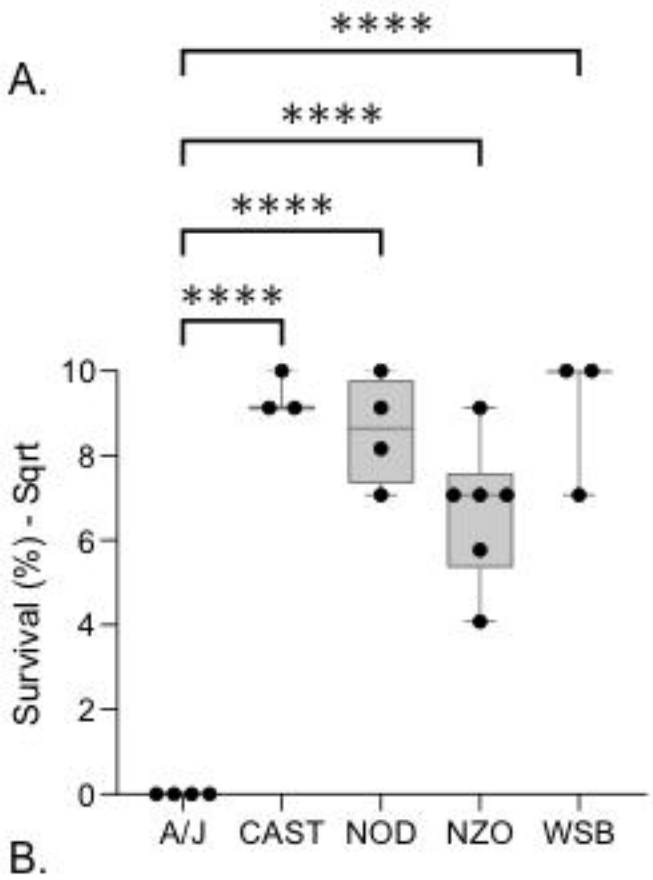

B.

GENE	SNP_ID	A/J	CAST	NOD	NZO	WSB	Cons
Uox	rs31217970	T	C	C	C	C	synonymous
Adgrl4	rs30505737	T	A	A	A	A	splice region
Ifi44	rs48866215	A.	G	G	G	G	missense
Ifi44l	rs31149902	G	A	A	A	A	synonymous
Miga1	rs31134017	G	T	T	T	T	missense
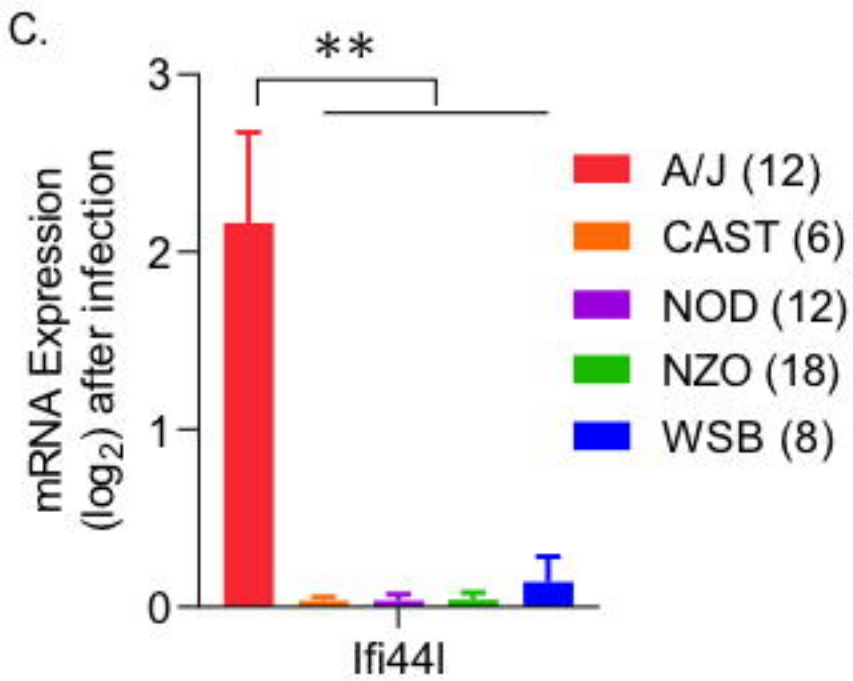
C.